AE-195
UDC 621.039.526
621.039.55

AE-195

Experimental Studies on Assemblies 1 and 2 of the Fast Reactor FRO

Part 1

T. L. Andersson, E. Hellstrand,
S-O. Londen and L. I. Tirén

AKTIEBOLAGET ATOMENERGI
STOCKHOLM, SWEDEN 1965

AE-195

EXPERIMENTAL STUDIES ON ASSEMBLIES 1 AND 2 OF THE FAST REACTOR FRO

PART 1

T.L. Andersson, E. Hellstrand
S-O. Londen and L.I. Tirén

Abstract

FRO is a fast zero power reactor built for experiments in reactor physics. It is a split table machine containing vertical fuel elements. 120 kg of U235 are available as fuel, which is fabricated into metallic plates of 20 % enrichment. The control system comprises 5 spring-loaded safety elements and 3 + 1 elements for start-up operations and power control.

The reactor went critical in February 1964. The first assemblies studied were made up of undiluted fuel into a cylindrical and a spherical core, respectively, surrounded by a reflector made of copper. The present report describes some experiments made on these systems. Primarily, critical mass determinations, flux distribution measurements and studies of the conversion ratio are dealt with.

The measured quantities have been compared with theoretical predictions using various transport theory programmes (DSN, TDC) and cross section sets. The experimental results show that the neutron spectrum in the copper reflector is softer than predicted, but apart from this discrepancy agreement with theory has generally been obtained.

Printed and distributed in August 1965.

LIST OF CONTENTS

1. Introduction

The present report contains an account of some experimental studies made on the first FRO assemblies. In this first part critical mass determinations, flux distribution measurements and studies of the modified relative conversion ratio are dealt with. In a second part of the report results will be given of reactivity measurements of different kinds such as control rod worths, void effects and reactivity equivalence of different materials. In a separate report by Häggblom [1] the theoretical calculations on the reactor are described and tables of the different cross section sets are given.

Whenever possible, the experimental results have been compared with calculated values. In many cases good agreement has been found. This is particularly true of conditions in the core itself. In the reflector large discrepancies exist in some cases, warranting further theoretical and experimental work. Some additional experiments are planned for the near future, but the results of these will be accounted for in later reviews of the FRO work.

The FRO machine is of the split table type containing vertical fuel and reflector elements (Fig. 1). The fuel element consists of a steel frame in two sections (Fig. 2) which are screwed together at the ends. The frame contains the parallel-epipedic fuel plates of uranium metal (20 % U235) and copper reflector plates. The fuel plates are 0.71 or 0.355 cm thick and most plates have a square section of 4.30 x 4.30 cm. The surface of the fuel is coated with a thin layer of teflon. With the dimensions used the core contains a minimum of 5.6 % of void and 6.5 % of stainless steel.

The reactor is furnished with three different types of regulating rods - five safety rods, three start rods and one fine control rod, all of them containing the pattern of core and reflector material appropriate to their position in the reactor. The safety rods are always in their "in" position during operation. The start rods are used for the approach to criticality when the two reactor halves have been brought together. Under normal operating conditions these rods are also in their "in" position. The positions of the rods in the first assembly are illustrated in Fig. 3.

The first cores studied consisted of undiluted fuel. The core was initially arranged into a circular cylinder with a height-to-diameter

ratio near 1. It was surrounded on all sides by a thick copper reflector. The core and reflector compositions and sizes are detailed in Table 2, section 3.3.

2. First approach to criticality

All positions in the core region not occupied by control rods were initially loaded with dummy elements filled with copper. These were subsequently replaced by elements containing fuel starting from the centre and proceeding outwards. In this way the core radius was gradually increased and criticality finally attained.

The stepwise loading of fuel was done with the reactor halves fully separated and the safety rods inserted in the system. After each loading step the reactor halves were driven together, the start rods raised into the core and count rates were measured on the pulse channels (BF_3 proportional counters). The location of the three detectors relative to reactor core and source position is shown in Fig. 4. Diagrams of inverse count rate versus fuel loading were plotted for all three channels and from these curves successive values of critical loading were estimated by extrapolation. Fig. 5 shows how the inverse count rate varied with fuel loading. The reactor went critical after the fourteenth loading step, the critical mass being 364.7 kg (cf. Table 1, section 3.2).

3. Measurements of critical mass

3.1 Introduction

Most of the experimental work was carried out with the fully reflected cylinder core. During the work it appeared that, altough the measured critical mass agreed well with theory, there were considerable discrepancies between experimental and theoretical flux distributions in the reflector (cf. sections 4 and 5). It was therefore considered worth while to make an experimental study of the dependence of the critical mass on reflector thickness to determine whether the agreement with theory was only fortuitous. With the limited fuel inventory of 600 kg it was not possible to reduce the reflector uniformly to zero thickness. The axial reflector thickness was therefore kept constant and the radial one was reduced gradually to a minimum of

6 cm, the corresponding uranium loading being 580 kg.

The fully reflected sphere (Assembly 2) was studied mainly on account of being more amenable to calculations than the cylindrical core.

The measurements of critical mass carried out on these systems will now be described and the results will be compared with theoretical predictions.

3.2 Corrections to loaded mass

After attaining criticality with a new core the loading was adjusted so as to make the system slightly supercritical with all control rods inserted. The excess reactivity was determined by a measurement of doubling time and the equivalent reduction in fuel mass was obtained by measuring the fuel-to-copper reactivity at the core-reflector boundary. Corrections were also made for the reactivity loss caused by the source access channel and the effect of the step irregularity at the core edge. In order to estimate the latter correction the fuel-to-copper reactivity measurements were extended to a number of radial positions in the vicinity of the core boundary. These data were used in a computer calculation with a programme which gives the irregular core to smooth core mass ratio [2]. In the measurements with reduced reflector thickness a similar edge correction was made for the outer reflector boundary to obtain effective reflector thicknesses.

Table 1, which refers to the first cylinder core, shows that the corrections are quite small.

Table 1: Corrections to loaded mass (Assembly 1)

Loaded mass, kg of uranium		365.9
Edge correction	x 0.9987	365.4
Fine control rod excess reactivity	34.7 pcm:	- 0.56
Source access channel reactivity	10.6 pcm:	- 0.17
Critical mass, kg of uranium		364.7

An investigation was also made of the possible error in the loaded mass itself, due to the small uncertainties in total fuel weight, teflon coating thickness and uranium enrichment. Of these factors only the last one proved to be significant. Measurements of the enrichment were carried out at two laboratories using mass spectroscopy technique; the average values obtained were 19.99 % and 20.10 % U235 by weight respectively. The variation in individual values obtained at each laboratory indicates an uncertainty of about ± 0.05 % U235 in both cases. An enrichment of 20.05 ± 0.05 % is therefore consistent with the measured values. The corresponding uncertainty in critical mass is of the order of 0.5 %, which is the limit of accuracy of the experimental critical mass determination.

3.3 Results and comparison with theory

The compositions of the core and reflector of the systems studied are given in Table 2 together with geometrical data for the fully reflected cylinder and sphere.

The measured and calculated critical mass values, expressed in kg U235, are listed in Tables 3 and 4. Before comparing the figures obtained, the calculational procedures will be considered briefly. For a more comprehensive account of the theoretical studies reference is made to the report by Häggblom [1].

Three computer programmes were available for the calculations:

A. The MUCC multigroup diffusion code [3] which approximates a two-dimensional solution by separation of variables. It is coded for the Ferranti Mercury Computer.

B. The one-dimensional DSN code [5] which solves the multigroup transport equation in spherical geometry using the Carlson S_N-method.

C. The two-dimensional TDC code [5] which also employs the Carlson S_N-method and is applicable to cylindrical geometry. In the version available at present this code cannot handle more than 6 energy groups.

Table 2: Data for FRO Assemblies 1 and 2

Core composition

Material	Volume per cent
Uranium[x]	87.7
U235[xx]	17.5(9)
U238	70.1(3)
Steel	6.5
Fe	4.8(1)
Ni	0.5(2)
Cr	1.1(7)
Teflon (CF_2)	0.2
Void	5.6

Reflector composition

Copper	88.5
Steel	6.5
Void	5.0

x Based on a density value of 18.87 g/cm^3

xx Enrichment = (20.05 ± 0.05) %

Fully reflected systems

	Cylinder (Assembly 1)	Sphere (Assembly 2)
Crit. mass kg U	364.7	350.3
kg U235	72.9	70.1
Core height, cm	30.1	-
Equivalent core radius, cm	15.3	17.2
Minimum reflector thickness, cm	34	35

The two latter codes, written for the IBM 7090 computer, were used as standard methods in spherical and cylindrical geometry, respectively, but some calculations with the MUCC diffusion code were also made for comparison (cf. below). The value of N used in the DSN and TDC codes was 4.

Initially all calculations were based on an 11-group cross section set compiled by Häggblom, which includes neutrons down to 1 keV (Set 1). The energy range was later extended to 120 eV, and new group cross sections for the whole energy range were obtained by weighting microscopic data with a fine-structure flux [1]. The number of groups chosen was 14 and 6. The cross sections of U238 and Cu were also reduced slightly as a result of new information. The ensuing group cross section sets will be denoted Set 2. The effect of these changes was a slight decrease in the calculated critical mass (Table 3, items 5 and 6). The group energy limits for the different sets are given in Table 5.

Table 3:

Fully reflected sphere (Assembly 2)

Item	Code	Cross section set	Crit. mass kg U235	Deviation from exp. %
1	DSN	Set 1, 11 groups	71.3	+ 1.7
2	DSN	Set 2, 14 groups	67.0	- 4.4
3	DSN	Set 2, 6 groups	66.3	- 5.3
4		Experiment	70.1	

Fully reflected cylinder (Assembly 1)

5	TDC	Set 1, 6 groups	73.6	+ 1.0
6	TDC	Set 2, 6 groups	71.0	- 2.7
		Experiment	72.9	

When using the TDC code 6-group cross section sets were used. The 6-group condensation of Set 1 proved to be somewhat inconsistent, giving about 4 % lower critical mass than the original 11-group set. This inconsistency is probably due to the fact that no fine-structure flux was available for weighting when the condensation was made. One should bear this in mind when comparing results obtained with the 6-group version of Set 1 with experimental values. The 6-group Set 2, on the other hand, gives only 1 % lower critical mass than the 14-group Set 2, as can be seen by comparing items 2 and 3 in Table 3.

In view of the considerable uncertainties in the cross sections the agreement between the calculated and measured values of critical mass for the fully reflected sphere and cylinder is satisfactory. One may also compare the values of the shape factor, i.e. M(sphere)/M(cyl.). The figure obtained from the measurements is 0.961 and from the calculations, items 3 and 6, 0.934. Since the latter figure should be insensitive to errors in the cross sections, the discrepancy indicates some inconsistency between the DSN and the TDC calculations in this case.

Table 4: Comparison of measured and calculated critical masses, kg U235

Reflector thickness cm	Experiment	TDC calculation x)	Deviation from exp. %
34.3	72.9	73.6	+ 1.0
18.3	78.4	78.4	0
15.1	82.2	81.5	- 0.9
12.4	86.8	85.2	- 1.0
10.6	90.8	88.4	- 2.7
7.3	102.0	99	- 3
6.0	107.8	106	- 2

x) by interpolation in Fig. 6

The values of critical mass obtained as a function of the side reflector thickness of the cylindrical core are contained in Table 4 and Fig. 6. The agreement between the experimental values and the TDC calculations is good. Since the 6-group Set I cross sections were used for the calculations the agreement in absolute values may be to some extent fortuitous, but the calculations show that the dependence of critical mass on reflector thickness is well represented by the TDC code.

The results as shown in Fig. 6 also demonstrate that the diffusion code MUCC is inadequate for an accurate calculation of the critical mass of a small, fast reactor like FRO.

In a separate experiment on the 34-cm side-reflector a change in critical mass with reflector thickness of about 0.02 kg U235 per cm of reflector was determined. Consequently the 34.3-cm reflector is nearly "infinite" in thickness and the notation "fully reflected" is appropriate to this system. This is also in accordance with theoretical results.

In the case of the thinnest reflectors back-scattering of epithermal neutrons from the surrounding steel structure and walls might have caused a slight decrease in critical mass, but the extent of this effect is unknown. The quoted accuracy of about 0.5 % in the measured critical mass values therefore only applies to the fully reflected systems.

Table 5: Group energy limits for the different group cross section sets used

Set 1, 6 groups		Set 2, 6 groups		Set 1, 11 groups		Set 2, 14 groups	
Group no.	Energy range MeV			Group no.	Energy range MeV		
1	1.35	-10.0	1.35 -10.0	1	2.25	-10.0	2.25 -10.0
2	0.5	-1.35	0.5 -1.35	2	1.35	-2.25	1.35 -2.25
3	0.18	-0.5	0.18 -0.5	3	0.825	-1.35	0.825 -1.35
4	0.067	-0.18	0.067 -0.18	4	0.5	-0.825	0.5 -0.825
5	0.0091	-0.067	0.0091 -0.067	5	0.3	-0.5	0.3 -0.5
6	0.001	-0.0091	0.00012-0.0091	6	0.18	-0.3	0.18 -0.3
				7	0.11	-0.18	0.11 -0.18
				8	0.067	-0.11	0.067 -0.11
				9	0.025	-0.067	0.025 -0.067
				10	0.0091	-0.025	0.0091 -0.025
				11	0.001	-0.0091	0.0055 -0.0091
				12			0.0021 -0.0055
				13			0.0005 -0.0021
				14			0.00012-0.0005

4. Reaction rate measurements

4.1 Introduction

In order to check the calculated multigroup spectra and group cross sections for the FRO assemblies 1 and 2, the reaction rates of a number of elements were studied at different radial and axial positions in the reactor. The fission rate measurements were made on an absolute scale using specially calibrated chambers. The following fissionable materials were used: U235, U238, Np237 and Pu239.

The foil activation measurements were mostly only relative in nature. The following reactions were studied: In115(n,n'), P31(n,p), Mn55(n,γ), Cu63(n,γ) and Au197(n,γ).

4.2 Fission chamber measurements

4.2.1 Calibration

The uranium and plutonium fission chambers were calibrated absolutely in a thermal flux, using the known percentages of U235 and Pu239, respectively, and a value of the thermal flux determined by β-γ coincidence measurements of activated gold foils.

The neptunium chamber was calibrated in relation to a U238 chamber using monoenergetic neutrons (4 MeV) from a Van de Graaff machine.

A more detailed description of the calibration will be published elsewhere [6].

4.2.2 Experimental arrangement

Measurements were made in narrow vertical channels through the core and the reflector. In this report results are given from measurements in the fully reflected cylindrical and spherical systems.

The channel through the fuel had a square cross section 7.1 x 7.1 mm^2. An aluminium tube, diam. 7.1, thickness 0.35 mm, was placed in the channel and a corresponding hole was drilled through the Cu reflector above the core (Fig. 7).

For the cylindrical assembly scans were made both in the axial (z) and radial (r) directions. The radial measurements were made by placing the vertical channels at different radial positions. The detector was always oriented vertically in the channel. Due to the geometry of the fission chamber (diam. and length of the sensitive electrode 3 mm and about 20 mm respectively (cf. Fig. 8)), the best resolution was obtained in the radial direction. Only the data from the radial distribution studies are included in this report.

For the spherical assembly measurements were made only in a vertical channel through the core centre.

The fissionable coatings in the chambers are electrodeposited, the thicknesses varying between 100 and 1000 $\mu g/cm^2$. Since the chamber walls are made of aluminium only 0.5 mm thick and we use teflon cable, the spectrum degradation due to the chamber and the cable was assumed to be negligible in comparison with the errors from the calibration [7].

4.3 Foil activations

Data for the different reactions used are given in Table 6.

Table 6:

Reaction	Threshold	Measured activity	Half life
In115(n,n')	1.5 MeV	γ 0.335 MeV	4.5 h
P31(n,p)	2.5 MeV	β	2.6 h
Mn55(n,γ)	-	β	2.6 h
Cu63(n,γ)	-	β	12.8 h
Au197(n,γ)	-	β	2.7 d

For both the cylindrical and spherical assemblies the foils were loaded in a central fuel element. Hence the measurements in the cylindrical assembly were made in the axial direction.

The foils were generally irradiated for some hours at a power level of about 5 Watts, corresponding to a central flux of about 6×10^8 n/cm^2, s. To avoid fission product contamination the foils were wrapped in thin aluminium foils during the irradiations.

4.4 Results

The experimental results are presented together with theoretical curves in Figs. 9 - 20.

In Figs. 9, 10, 16 and 17 the fission rates from the fission chamber measurements are shown. The theoretical curves and the experimental measurements are normalized to 1 at the core centre. Since the fission rates were measured absolutely, the spectrum sensitive fission ratios $\left(\frac{U238}{U235}\right)_f$, $\left(\frac{Np237}{U235}\right)_f$ and $\left(\frac{Pu239}{U235}\right)_f$ could be obtained. They are shown in Figs. 18 - 20.

The results from the foil activations are given in Figs. 11 - 15. As for the fission rates the curves have been normalized to 1 at the core centre.

4.5 Theoretical reaction rates

The theoretical reaction rates shown by the curves in the diagrams were calculated from the 6-group TDC and 14-group DSN spectra, discussed

in section 3.3 and [1]. For the 6-group calculations the group division given in column 1 of Table 5 was used. The group cross sections for the reactions U235(n,f), U238(n,f) and Pu239(n,f) were calculated by Häggblom [1],[8]. The Np237(n,f) cross section set was taken from [9]. For the other reactions the cross section sets were constructed from primary microscopic cross section data using the NESPECO program [4]. The primary data were in these cases mainly taken from the references given in Table 7.

Table 7:

Reaction	Reference
In115(n,n')	[10]
P31(n,p)	[10], [11], [12]
Mn55(n,γ)	[13], [14]
Cu63(n,γ)	[8], [10], [15]
Au197(n,γ)	[16], [17], [18]

4.6 Discussion

The threshold reactions used are given in Table 8.

Table 8:

Reaction	Threshold Energy MeV (approx.)
U238(n,f)	1.4
Np237(n,f)	0.7
In115(n,n')	1.5
P31(n,p)	2.5

For these reactions good agreement is obtained between experiment and theory over the entire core and reflector, as seen in Figs. 9, 10 and 12. This indicates that the spatial distribution of the high energy neutron flux is well predicted by theory.

For the non-threshold reactions the agreement with theory is less

good, as shown in Figs. 13 - 17. The calculated reaction rates are too low, especially in the reflector. The discrepancy is larger the more sensitive the reaction is to low energy neutrons. For the Mn55(n,γ) reaction (Fig. 15), where the disagreement is largest, the main contribution to the reaction rate far out in the reflector comes from the resonance at 330 eV. The calculations apparently predict far too few low energy neutrons.

The spatial variation of the Cu63(n,γ) reaction rate differs considerably from that of the Mn55(n,γ) and Au197(n,γ) rates. The peaks shown by the latter two are completely missing for the former. This is, at least partly, due to resonance self-shielding in the copper reflector. To demonstrate the shielding effect experimentally, the following measurement was made in Assembly 2. Copper and gold foils were loaded at different positions in the top reflector. Corresponding foils were placed in symmetrical positions in the bottom reflector. A piece of natural uranium about 7 mm thick was loaded above and below each of these latter foils.

The effect of the uranium is twofold. Firstly, there will be a slight overall decrease in the neutron flux due to the increased absorption. Secondly, the dips in the reflector spectrum due to the copper resonances will be smoothed out by scattering events in the uranium. This effect should be well pronounced at the foil positions between the uranium plates. It should therefore be expected that, for these foils, the gold activity should be somewhat lower and the copper acitivty higher than at the corresponding positions in the top reflector. As illustrated in Figs. 13 and 14, this result is also borne out by the experiment. In Fig. 13 the directly measured copper data are given together with the reaction rates normalized to the same gold activity.

The self-shielding effect in copper has been demonstrated previously by Leipunski et al. [19]. In those experiments nickel was placed around the copper foils. The use of uranium for these preliminary self-shielding studies was motivated by the additional experiments discussed in the next section.

The experimental and theoretical fission ratios $\frac{U238}{U235}$, $\frac{Np237}{U235}$ and $\frac{Pu239}{U235}$ agree within the limits of experimental error in the central parts of the system. In the outer parts of the core and in the reflector, however, all three ratios are calculated too high, giving additional

evidence of a too hard theoretical spectrum (Figs. 18 -20). This is particularly true for the 6-group calculations but the difference remains when 14 groups are used. It must be noticed that there is a rather large uncertainty also in the theoretical $\frac{Np237}{U235}$ curve due to the lack of accurate fission cross section data for neptunium.

If the rough assumption is made that the only error in the calculated spectrum is that the group fluxes Φ_{11}, Φ_{12}, Φ_{13} and Φ_{14} are too low by a common factor, then it can be estimated how much larger these group fluxes must be to give agreement between the theoretical and experimental curves in, for instance, Fig. 16. It is found that in the reflector Φ_{11}, ..., Φ_{14} must be multiplied by factors between 4 (just outside the core) and 30 (in the outer parts of the reflector), indicating a strongly increased softening of the spectrum with increasing distance from the core. This can also be seen from the Mn55(n,γ) curves in Fig. 15, where the theoretical curve (14-group calculation) has the peak at a radius of about 200 mm but the experimental curve has the corresponding peak at about 300 mm. Room-reflected neutrons might be of some significance in the outer part of the reflector but, as discussed in the next section, they are assumed to be of minor importance at the positions just mentioned.

The cross section data for the reflector (copper) are rather uncertain, especially for energies below 10 keV. To investigate the sensitivity of the calculated group fluxes to the low energy cross sections, calculations were made with somewhat changed input data for this energy region. In our series of calculations the capture cross section in group 14 was reduced from 0.015 cm^{-1} to 0.002 cm^{-1}. This gave an increase in Φ_{14} by a factor of 2 but a slight decrease in the preceding groups.

In another calculation the down-scattering cross sections $\Sigma_{3\to8}$, $\Sigma_{3\to9}$, ..., $\Sigma_{3\to14}$ were all increased by a certain amount, 0.002 cm^{-1}, corresponding to about 40 % increase in the total inelastic scattering cross section. This change caused an increase by a factor of about 1.5 in Φ_{11}, ..., Φ_{14}.

The changes obtained for the low energy fluxes do not substantially improve the agreement between the experimental and calculated reaction rates under discussion. Further variations in the cross

sections must be made in the future, supplemented by additional experimental studies of background effects etc.

5. Conversion ratio measurements

5.1 Introduction

The measured quantity was the "modified relative conversion ratio" defined as

$$RCR^{*} = \frac{\left[\frac{\text{U238 capture}}{\text{U235 fission}}\right] \text{(FRO spectrum)}}{\left[\frac{\text{U238 capture}}{\text{U235 fission}}\right] \text{(thermal spectrum)}}$$

From this quantity the true conversion ratio in the fast spectrum, i.e. $\left[\frac{\text{U238 capture}}{\text{U235 absorption}}\right]$, can be found using tabulated thermal cross sections and a calculated value of the capture-to-fission ratio of U235.

A more detailed account of the measurements summarized here is given in [20].

5.2 Irradiations

Irradiations were made in the FRO core and reflector and in the thermal column of the R1 research reactor. In both experiments natural uranium foils, 0.05 or 0.13 mm thick, were placed close to a small fission chamber containing U235 and irradiated for several hours at a constant power level. The fission chamber was of the same type as shown in Fig. 8. In the thermal irradiation, which was carried out less than 24 hours before or after the FRO irradiation, a slight flux depression occurs in the natural uranium foils, but apart from this effect it was assumed that the foils and the chamber were exposed to the same neutron flux and that no spectrum perturbation was caused by the small amounts of material introduced.

5.3 Determination of U238 capture rate

The capture rate in U238 was detected by counting the Np239 γ-activity of the irradiated foils, using the γ-X coincidence technique.

Since many accounts of this method are available [21, 22, 23] in the literature, the general principles need no further presentation. A block diagram of the fast/slow coincidence unit used at the FRO reactor is shown in Fig. 21.

The apparatus includes a channel for detection of fission product activity. The output from one of the linear amplifiers is connected to a discriminator, which is set at a suitable level so as to accept fission product gammas only. These pulses are accumulated in the FP-scaler shown in the figure.

An automatic sample changer is attached and the data obtained are punched on tape. Data reduction is performed by means of the KODAK program [24].

A highly enriched U235 sample irradiated in a thermal spectrum was used as a "fission product monitor", by means of which a correction for the fission product activity in the natural uranium samples could be made. As regards samples irradiated in a fast spectrum, however, the latter activity originates partly from U238 fissions; hence a systematic error is present due to differences in the decay curve of the U238 and U235 fission products. For this reason it is desirable that the fission product correction be as small as possible even if it can be measured with high statistical accuracy.

Using the coincidence method the correction was of the order of 1 - 2 % in the case of the fast spectrum irradiation, and 5 to 10 times larger with single-channel counting.

5.4 Measurements of U235 fission rate

The measurements of the U235 fission rate by means of the fission chamber were limited to determining the FRO-to-R1 counting rate ratio for the central position in FRO. Information regarding the spatial distribution of the fission rate was avialable from the measurements reported in section 4.

Since fission counts were accumulated during the whole irradiation experiment, the statistical error was very small (less than 0.1 %). The largest uncertainty in these measurements arises from dead time losses at the thermal irradiation and amounts to max. ± 0.2 %.

The fission rate was alternatively measured by counting fission product γ-rays from irradiated foils containing U235. In the latter method, however, a systematic error appeared when comparing the activity in samples irradiated in the fast (FRO) and the thermal spectrum. This error can be explained as due to the variation in the yield figures for the fission products with the energy of the neutron causing the fission.

5.5 Results and comparison with theory

5.5.1 Measurements at core centre

The numerical value of RCR^* obtained at the centre of the core is given in Table 9 together with theoretical results. For reasons given above the runs using fission foils were excluded. The margin of error shown includes counting statistics and other random effects as well as uncertainties due to dead time in the fission counting channel and flux depression in the foils irradiated in the thermal column.

In order to compare the measured value with a theoretical estimate, the capture-to-fission ratios were calculated using for the thermal spectrum (T_n = 20 °C).

$\sigma_f(25)$ = 578 b [25]

$g_f(25)$ = 0.976 [26]

$\sigma_c(28)$ = 2.71 b [10]

The effective cross sections in the FRO core were calculated using the DSN code and various cross section sets. The theoretical values are about 4 % higher than the experimental figure. This difference can probably be attributed to cross section uncertainties, particularly in the U238 capture cross section.

Table 9:

Type of calculation	Cross sections set	Result, RCR^* core centre
DSN 14 groups	Häggblom [1]	22.6
DSN 16 groups	Y.O.M. [27]	22.4
DSN 16 groups	Hansen & Roach [28]	22.8
	Experiment	21.65 ± 0.17

5.5.2 Spatial distributions

The axial and radial distributions of the U238 capture rate in assembly 1 are shown in Figs. 22 and 23 and the corresponding distribution in spherical geometry (assembly 2) in Fig. 24. The points are normalized at the centre and the accuracy of each point is between 0.5 and 1 %. The presence of a peak in the capture rate in the reflector near the core boundary is particularly noteworthy. This behaviour has so far not been reproduced properly in the theoretical curves which are also shown in the figures. The 6-group calculation (column 1, Table 5) of Fig. 22 was made with the TDC code. While the theoretical curve is in good agreement with the experiment in the major portion of the core, there is a large discrepancy in the reflector. The result obtained in the spherical case (Fig. 24) by means of the DSN code is similar. Here the Hansen-Roach cross section set was used, which covers neutron energies down to thermal.

The adjustment of the copper cross sections discussed in section 4 only had a marginal effect on the calculated curve. Nor was it possible to bring the curves together by any reasonable change in the U238 capture cross section.

Resonance shielding effects make the effective U238 cross section different in the core and the reflector. In order to study these effects, uranium foils were included in the copper and gold foil packages which were irradiated with and without uranium around them (cf. section 4.6). By normalization to the gold activity the overall flux depression due to the uranium plates - as distinct from the resonance flux depression - could be corrected for. The capture rate in the shielded foils (Fig. 24) is strongly reduced relative to the unshielded ones; consequently a large portion of the capture takes place in the resonance region below 1 keV.

In the Hansen-Roach cross section set the group cross sections can be obtained for any degree of resonance self-shielding. The theoretical curves corresponding to the shielded and unshielded arrangements were nearly identical, however. It may therefore be concluded - as in section 4 - that the calculated spectrum is too hard.

It was suggested that the numerous low energy neutrons are due to back-scattering from the walls of the reactor hall. A simple experiment was made to estimate the extent of back-scattering radiation, using a He-3 proportional counter as detector. It appeared that the flux is approximately isotropic at a distance of 30 cm from the outer edge of the side-reflector and the inward current on the reflector amounts to about 10 % of the flux at a point in the reflector 16 cm from the core boundary. It is therefore likely that a correction for back-scattered neutrons would lower the experimental curves appreciably in the outer part of the reflector but the correction would be small compared with the difference between the experimental and theoretical curves.

The spatial distribution of the U238 capture/U235 fission ratio was obtained using the results discussed above in combination with fission chamber scans by Andersson (section 4). The result, in terms of a local conversion ratio, is shown in Fig. 25 for the spherical core together with a calculated curve (DSN, 14 groups). The experimental result shows that there are only small changes in the spectrum out to a distance from the core centre of about 11 cm. In the reflector, on the other hand, there is a continuing spectrum-softening which is not shown in the theoretical curve.

Acknowledgements

We should like to thank Dr. H. Häggblom for many stimulating discussions. We also wish to express our gratitude to Å. Klingfeldt, J-C. Lupander, H. Öhman and the members of the FRO operations team for valuable technical assistance.

References

1. HÄGGBLOM, H,
Theoretical work for the fast zero-power reactor FRO.
1965 (AE-194).

2. AHLIN, Å and TIRÉN, L I,
AB Atomenergi, Sweden, Internal reports (RFX-331 and FFX-16).

3. LINDE, S,
The multigroup neutron diffusion equations/1 space dimension.
1960 (AE-35).

4. HÄGGBLOM, H and NYMAN, K,
AB Atomenergi, Sweden, Internal report (RFN-173) (In Swedish).

5. CARLSON, B et al.,
The DSN and TDC neutron transport codes.
1959 (LAMS-2346).

6. ANDERSSON, T L,
To be published as AE-report.

7. DAVEY, W G and CURRAN, R N,
An experimental investigation of some sources of error in the measurement of absolute fission ratios in fast reactors.
1961 (ANL-6468).

8. HÄGGBLOM, H,
Private communication, 1964.

9. MICHAEL, P,
Theoretical analysis of the exponential experiment in natural uranium.
Nucl. Sci. Eng. 18 (1964) 130-136.

10. HUGHES, D J and SCHWARTZ, R B,
Neutron cross sections.
1958 (BNL-325 2 ed.).

11. CUZZOCREA, P et al.,
Cross section for P31(n, p)Si31 reaction up to 5 MeV.
Nuov. Cim Ser. 10, 16 (1960) 450-456.

12. GRUNDL, J A et al.,
P31(n, p)Si31 and Al27(n, α)Na24 cross sections.
Phys. Rev. 109 (1958) 425-428.

13. TROUBETZKOY, E S et al.,
Fast neutron cross section of manganese, calcium, sulfur and sodium. Final report 1 Dec. 1959 - 31 Dec. 1960.
1961 (NDA 2133-4).

14. STAVISSKII, Yu Ya and TOLSTIKOV, V A,
Radiative capture cross sections of Mn55, Cu65, Ba138 and Th232 for 0.03 - 2 MeV neutrons.
Atomnaya Énergiya 10 (1961) 508-511.

15. STAVISSKII, Yu Ya and SHAPAR, A V,
Fast-neutron capture cross section values of copper and zirconium.
Atomnaya Énergiya 15 (1963) 323.

16. BARRY, J F,
The radiative capture cross section of Au197 for neutrons in the energy range 0.12 - 1.8 MeV.
Journ. of Nucl. Energy parts A/B 18 (1964) 491-496.

17. BERGQVIST, I,
Fast neutron radiative capture cross sections in Ag, Ta, W, Au, Hg and U.
Ark. Fys. 23 (1963) 425-434.

18. NEILER, J H,
Neutron capture cross sections for energies above a few hundred electron-volts.
Physics of fast and intermediate reactors. Proc. of the IAEA seminar held in Vienna 1961, Vol 1, Vienna 1962, p. 105.

19. LEIPUNSKY, A I et al.,
Studies in the physics of fast neutron reactors,
2nd United Nations International Conference on the Peaceful Uses of Atomic Energy, Geneva 1958. Proceedings, Vol 12, Geneva 1958, p. 3-15.

20. TIRÉN, L I and LUPANDER, J C,
AB Atomenergi, Sweden, Internal report (FFX-10).

21. SHER, R,
Gamma-gamma Coincidence Method for Measuring Resonance Escape Probability in U238 Lattices.
Nucl. Sci. & Eng. 7 (1960) 479-480.

22. WEITZBERG, A et al.,
Measurements of Neutron Capture in U238 in Lattices of Uranium Rods in Heavy Water.
1962 (NYO-9659).

23. TUNNICLIFFE, P R et al.,
A Method for an Accurate Determination of Relative Initial Conversion Ratios.
Nucl. Sci. & Eng. 15 (1963) 268-283.

24. AHLIN, Å et al.,
AB Atomenergi, Sweden, Internal report (FFX-4).

25. WESTCOTT, C H et al.,
Survey of Nuclear Data for Reactor Calculations.
1964 3rd International Conference on the Peaceful Uses of Atomic Energy, Geneva 1964 (A/Conf. 28/P/717).

26. WESTCOTT, C H,
Effective Cross Section Values for Well-Moderated Thermal Reactor Spectra, (3 ed., corr.).
1960 (AECL-1101, CRRP-960).

27. YIFTAH et al.,
Fast Reactor Cross Sections.
Oxf. Pergamon Press (1960).

28. HANSEN, G E and ROACH, W H,
Six and Sixteen Group Cross Sections for Fast and Intermediate Critical Assemblies.
1961 (LAMS-2543).

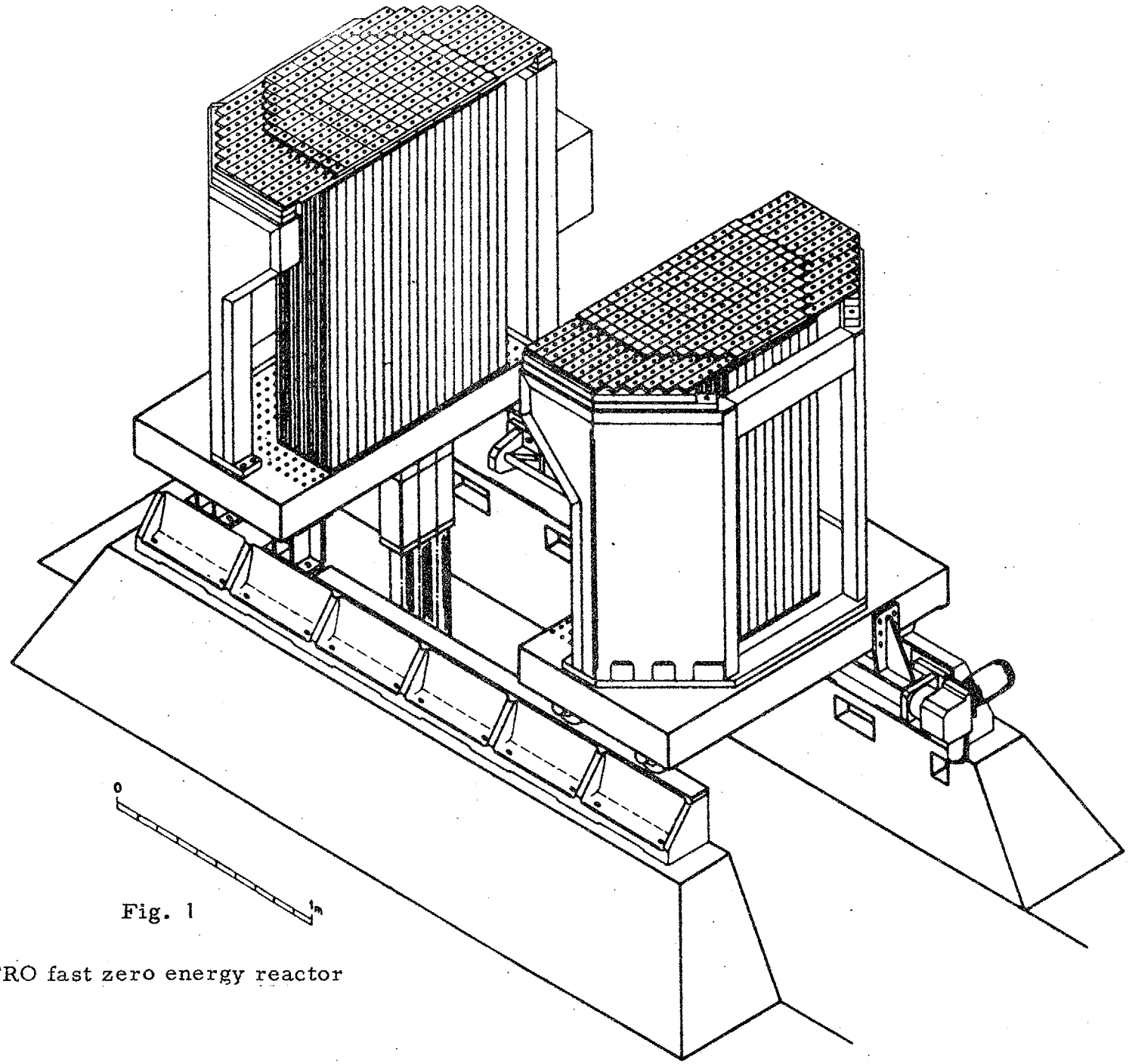

Fig. 1

FRO fast zero energy reactor

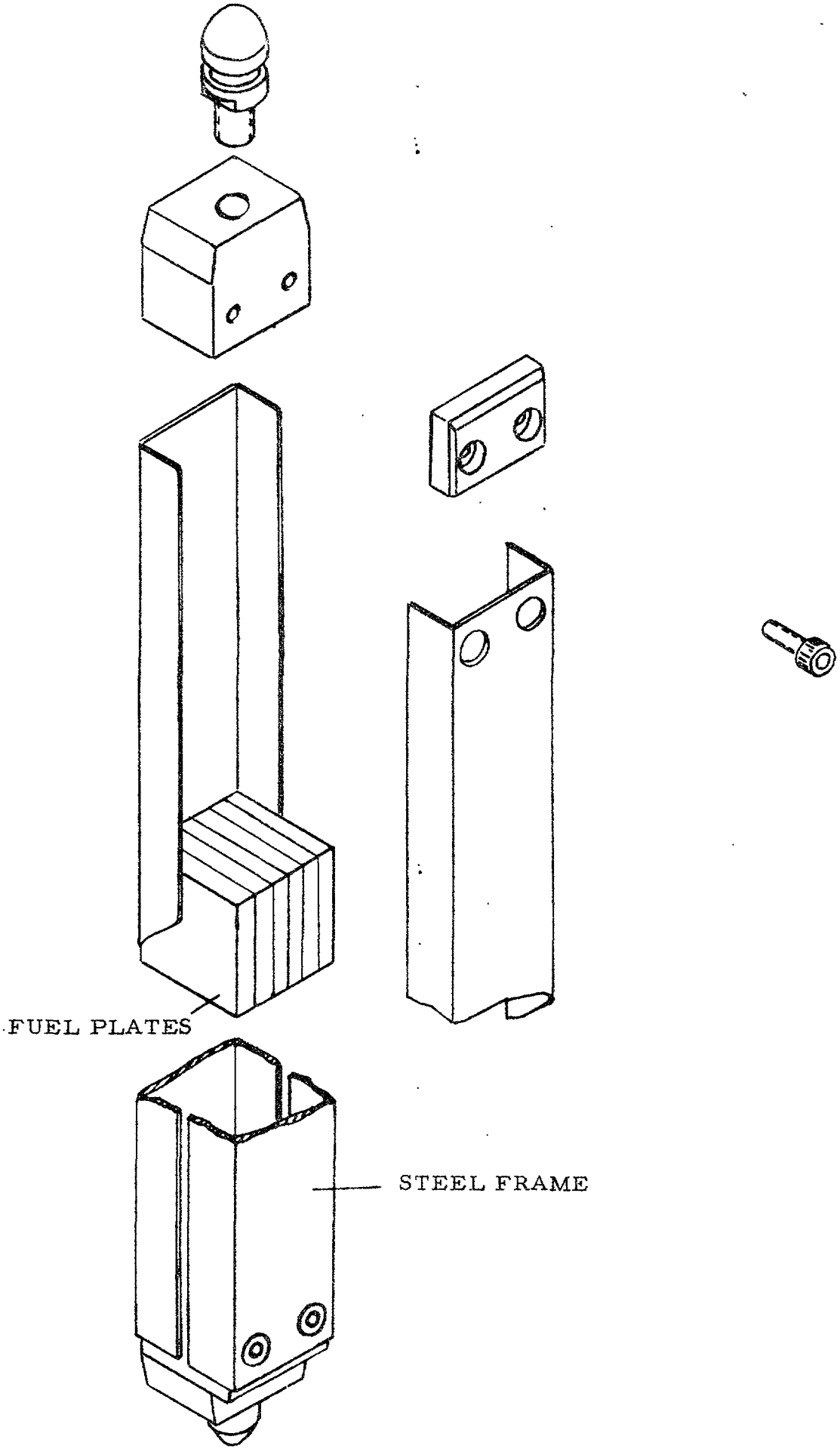

Fig. 2

FRO fuel element

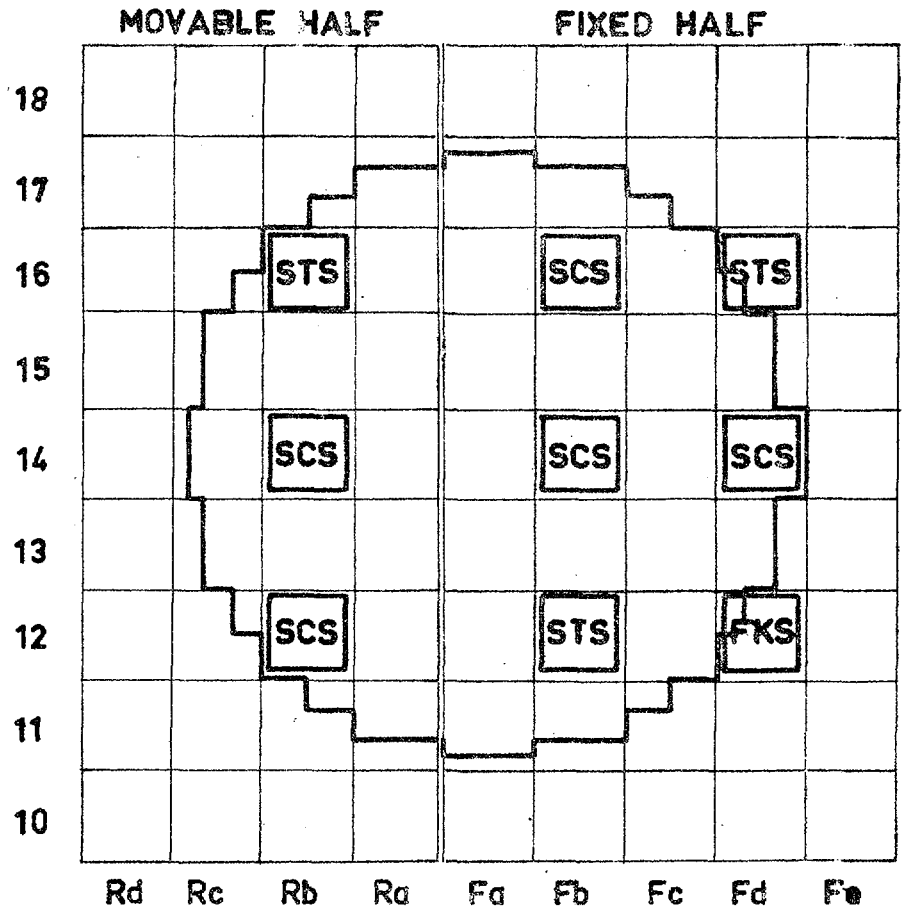

SCS = Safety rod

STS = Start rod

FKS = Fine control rod

Fig. 3

Loading pattern for assembly 1

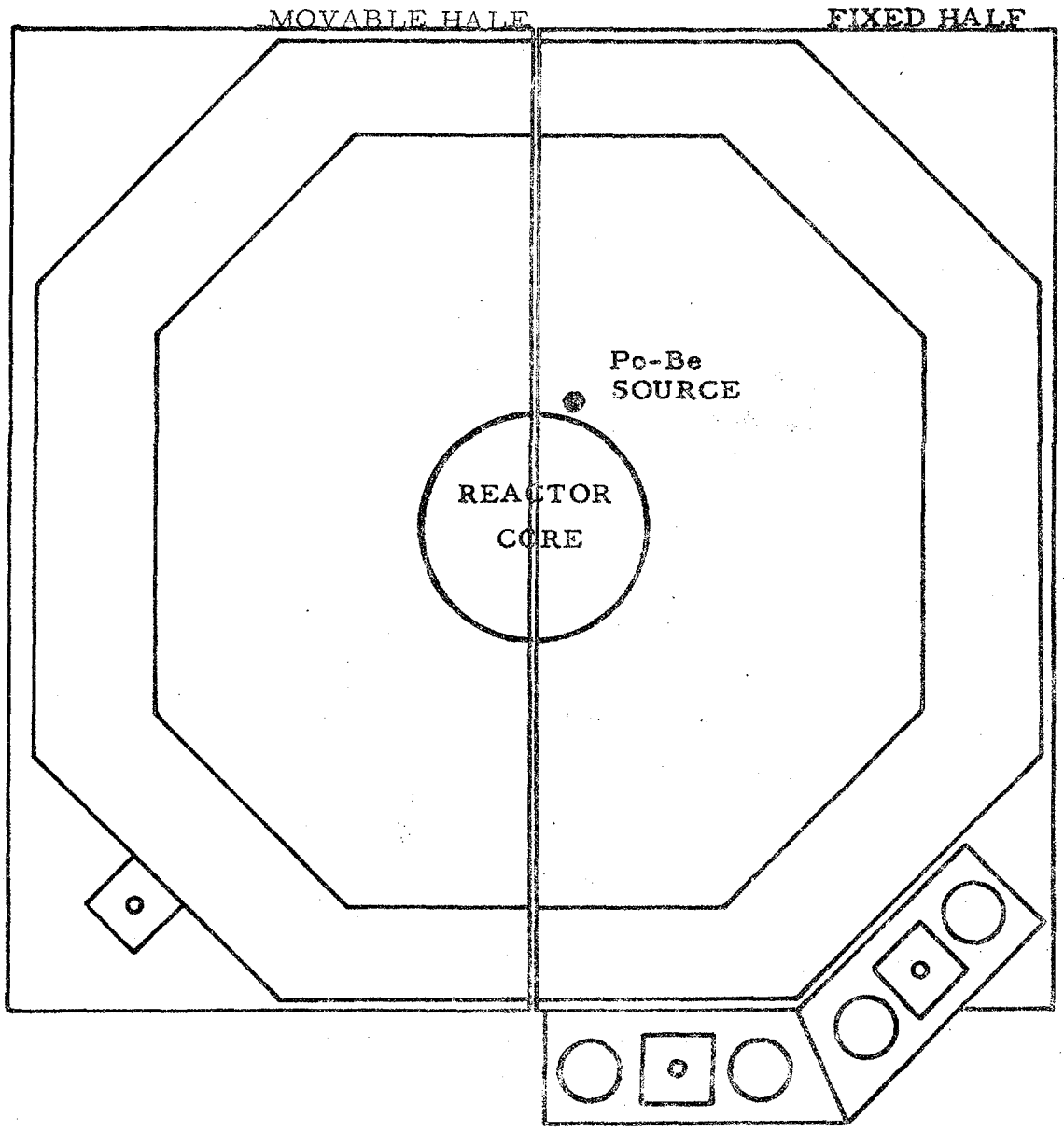

Fig. 4

Nuclear instrumentation and source arrangement

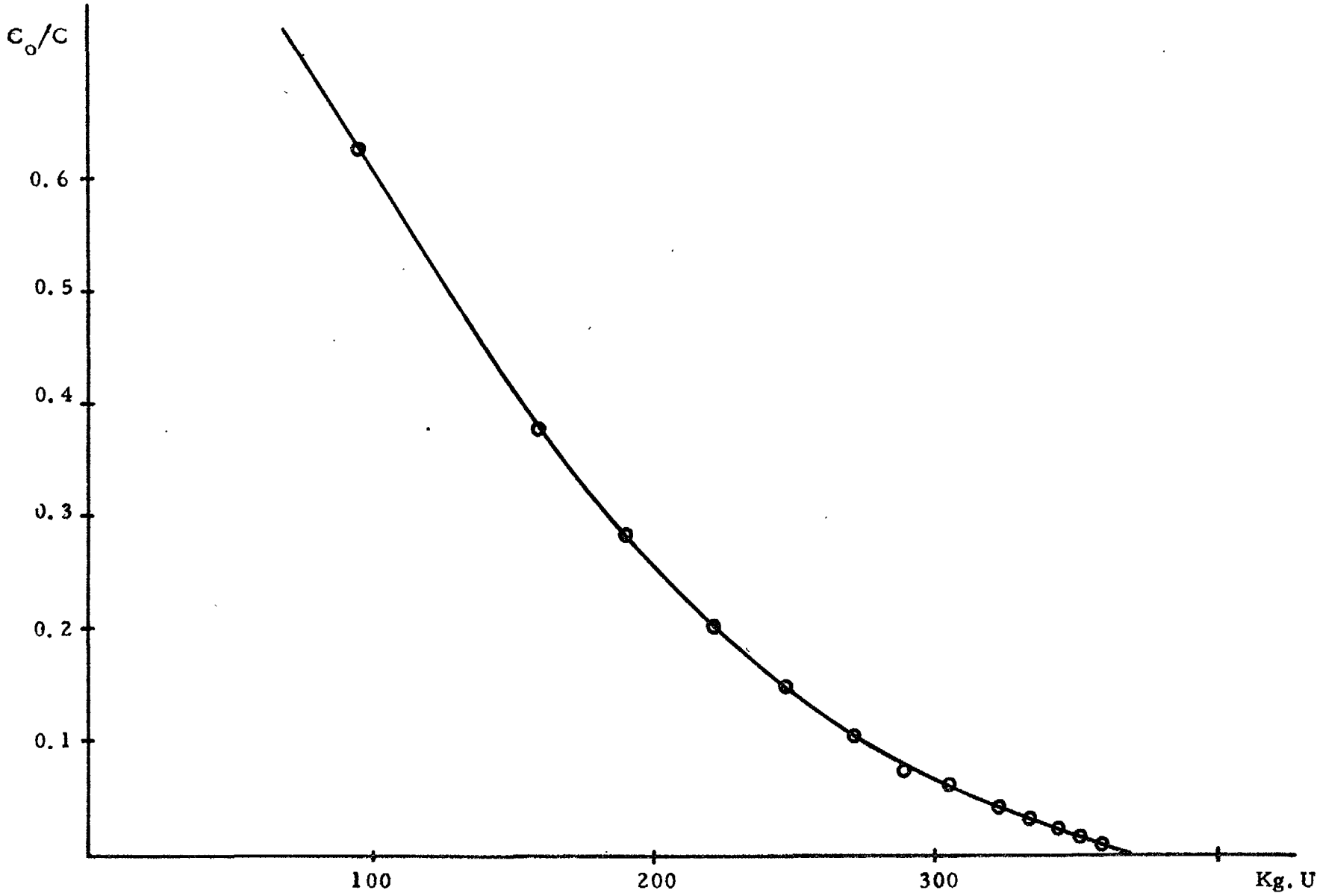

Fig. 5

Inverse multiplication curve

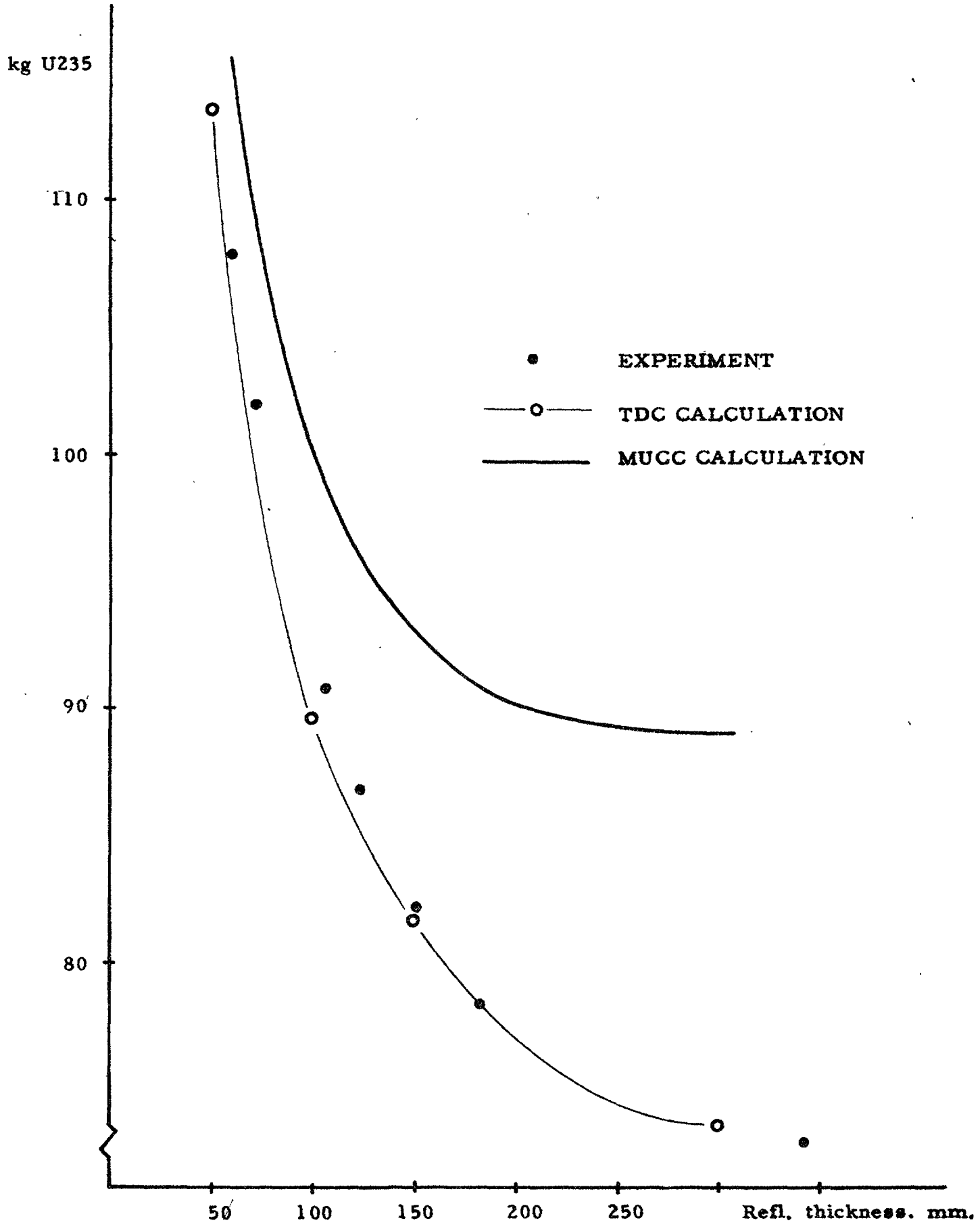

Fig. 6

Critical mass versus side reflector thickness

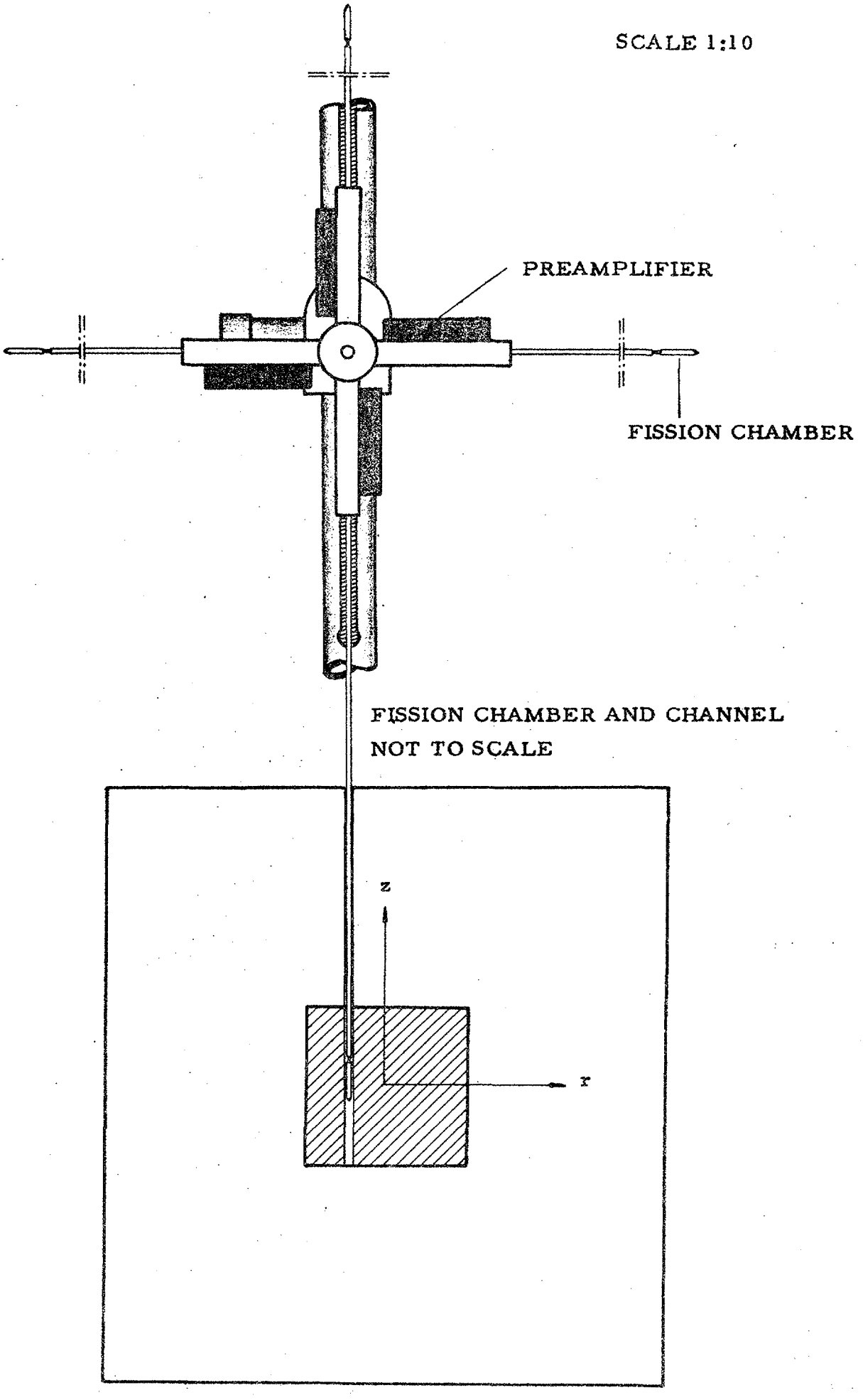

Fig. 7

Experimental arrangement for fission chamber scans

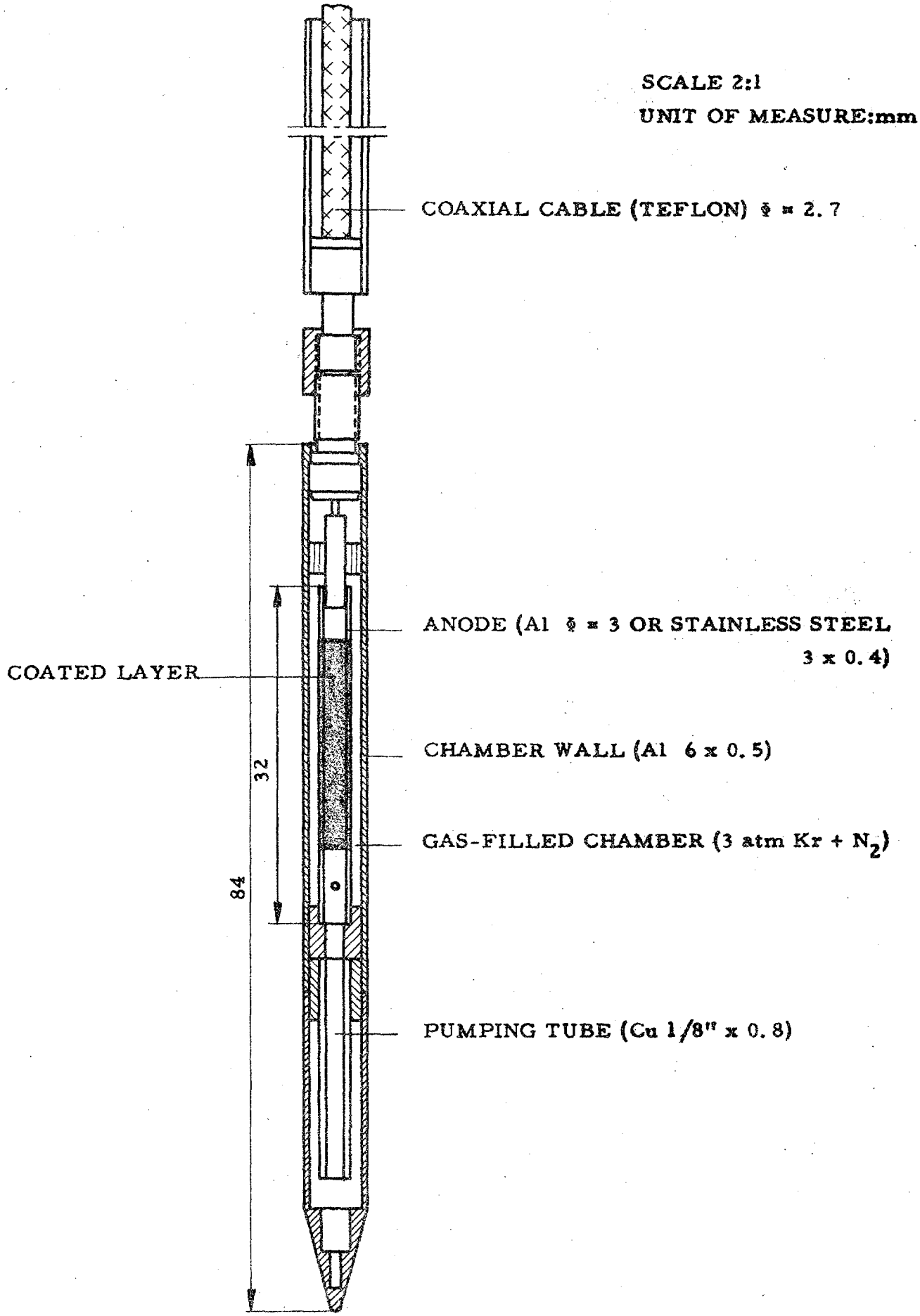

Fig. 8

Fission chamber

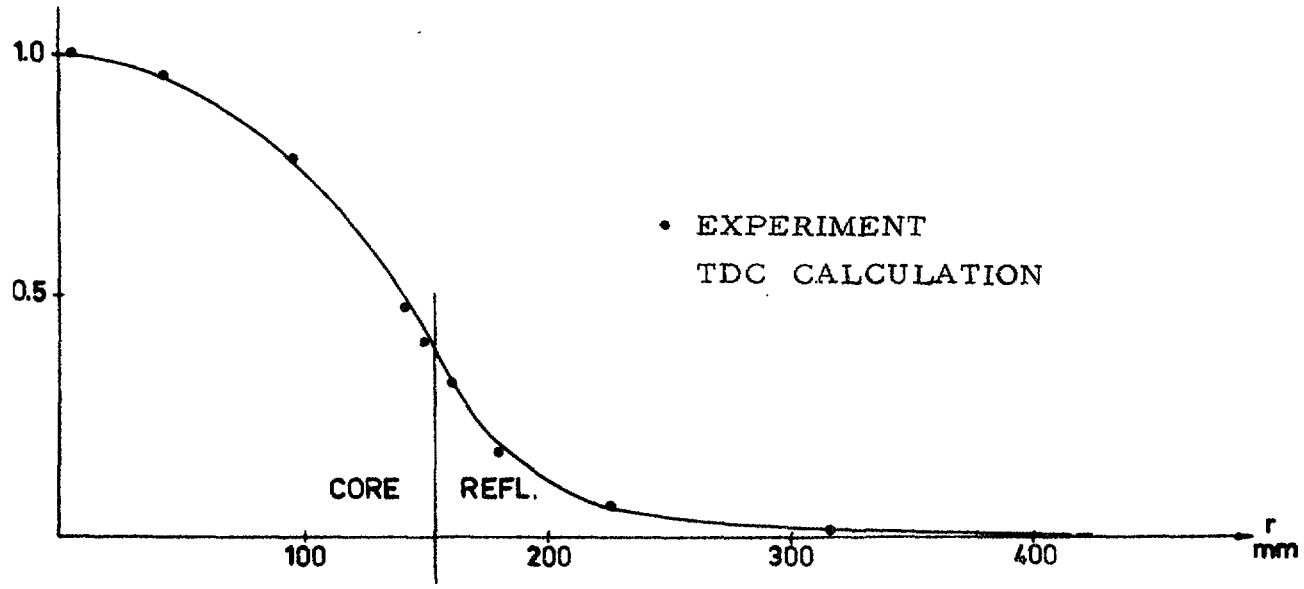

ASSEMBLY 1

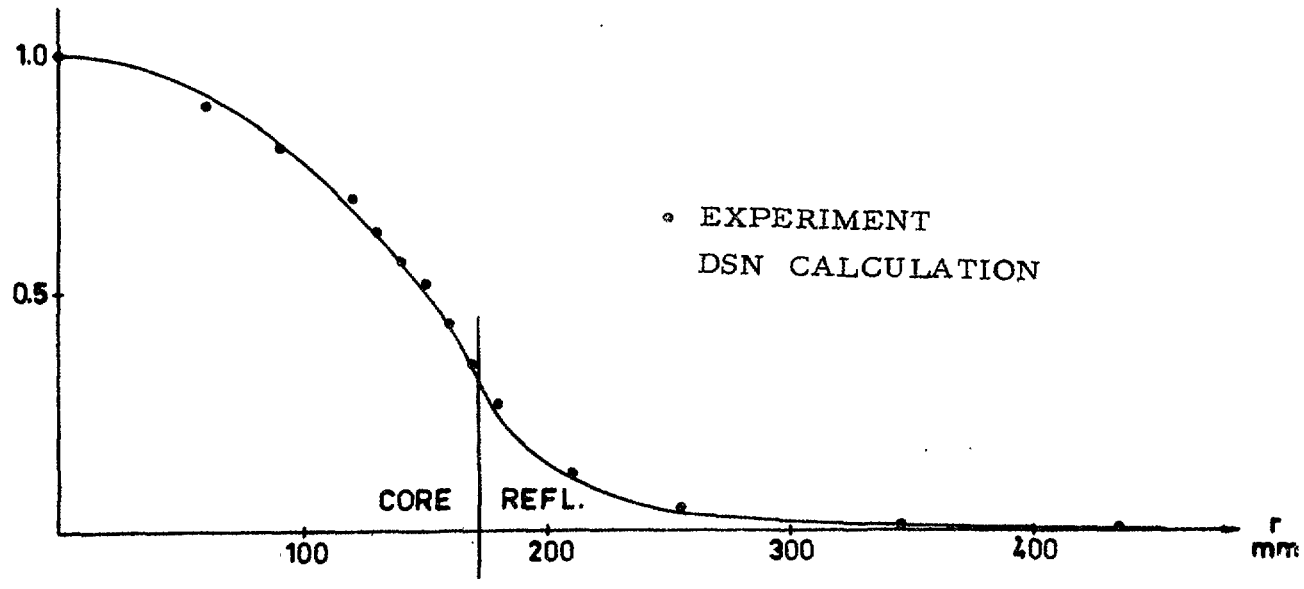

ASSEMBLY 2

Fig. 9

U238 fission rate, radial distribution

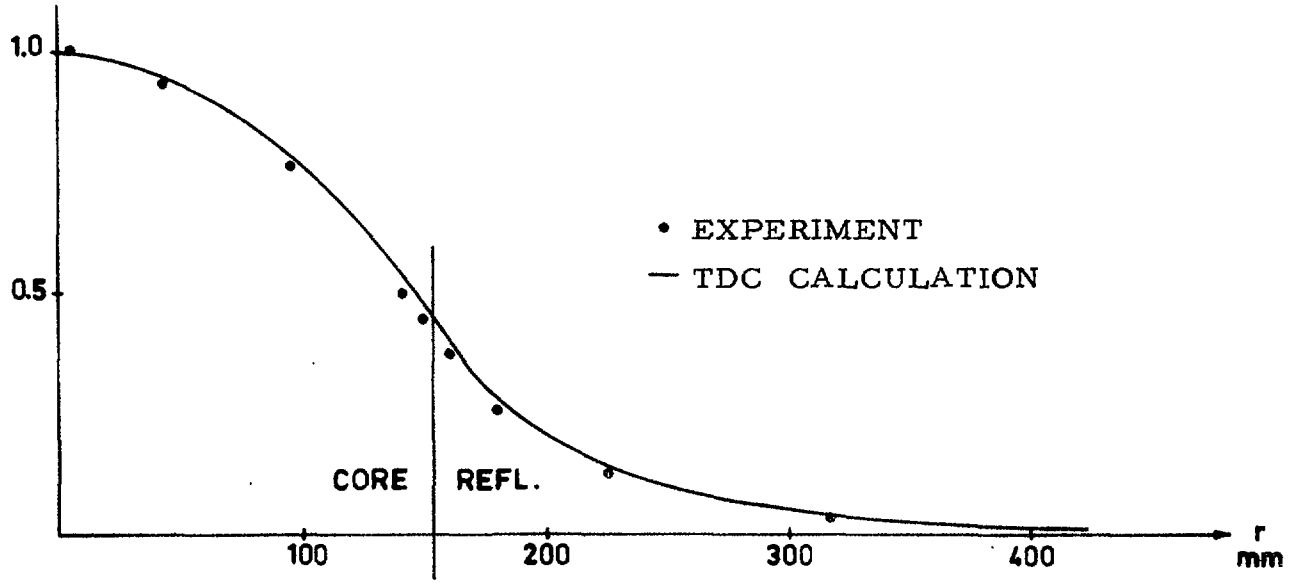

ASSEMBLY 1

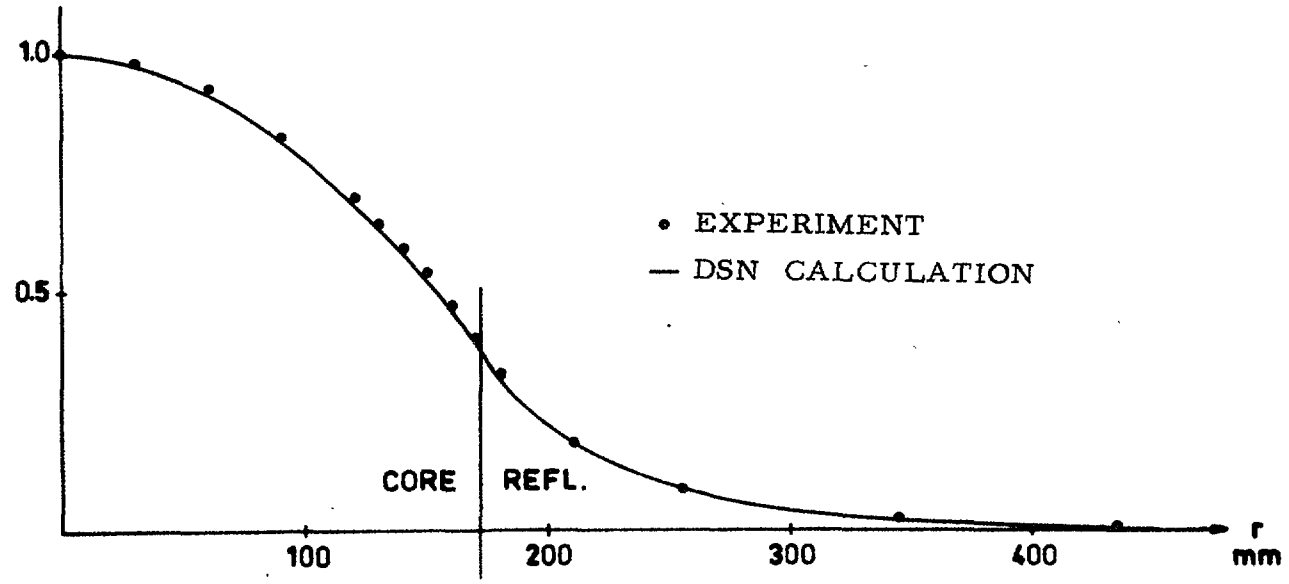

ASSEMBLY 2

Fig. 10

Np237 fission rate, radial distribution

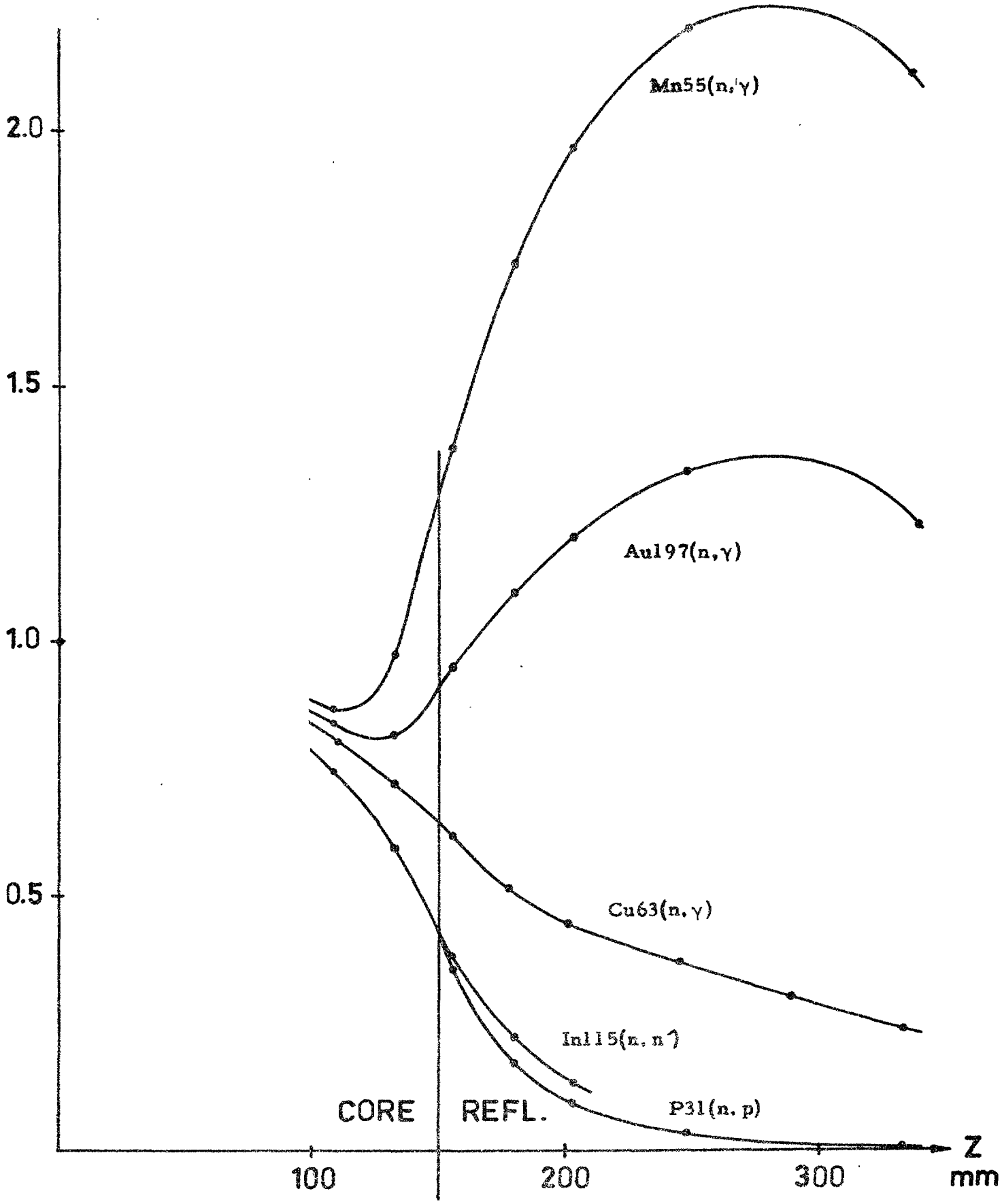

Fig. 11

Reaction rates as measured by foil activation,
axial distribution in assembly 1

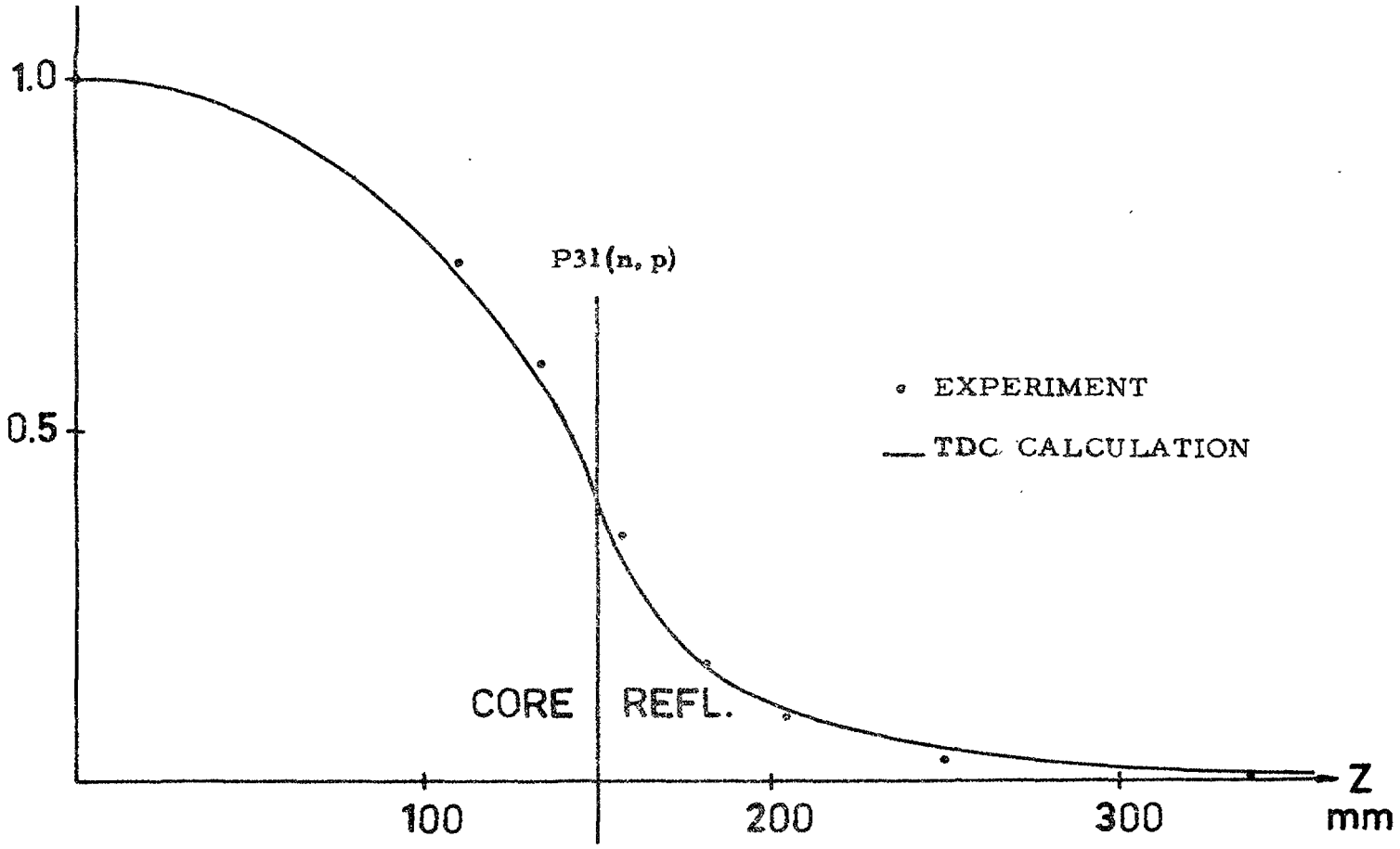

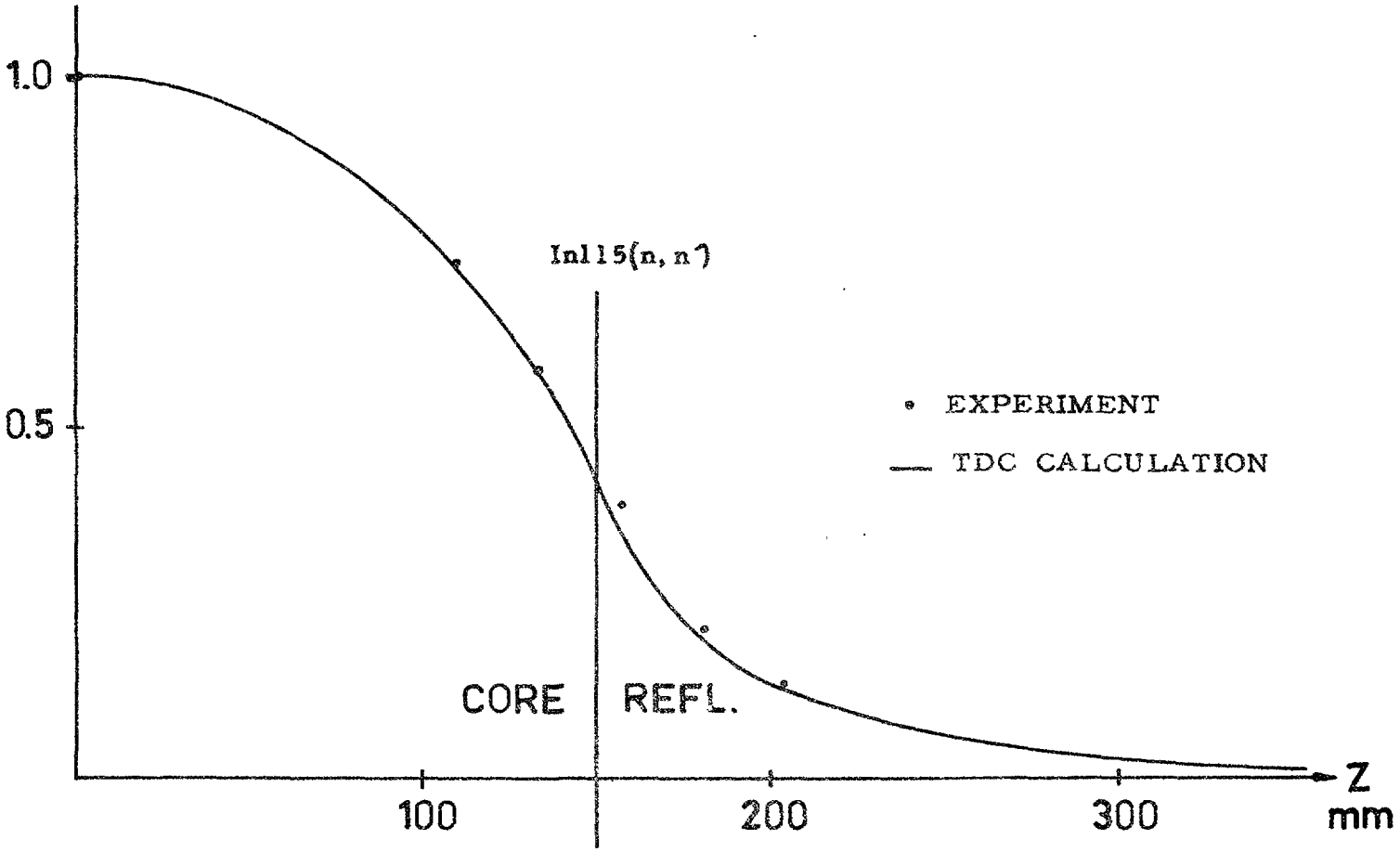

Fig. 12

P31(n, p) and In115(n, n') reaction rates, axial distribution in assembly 1

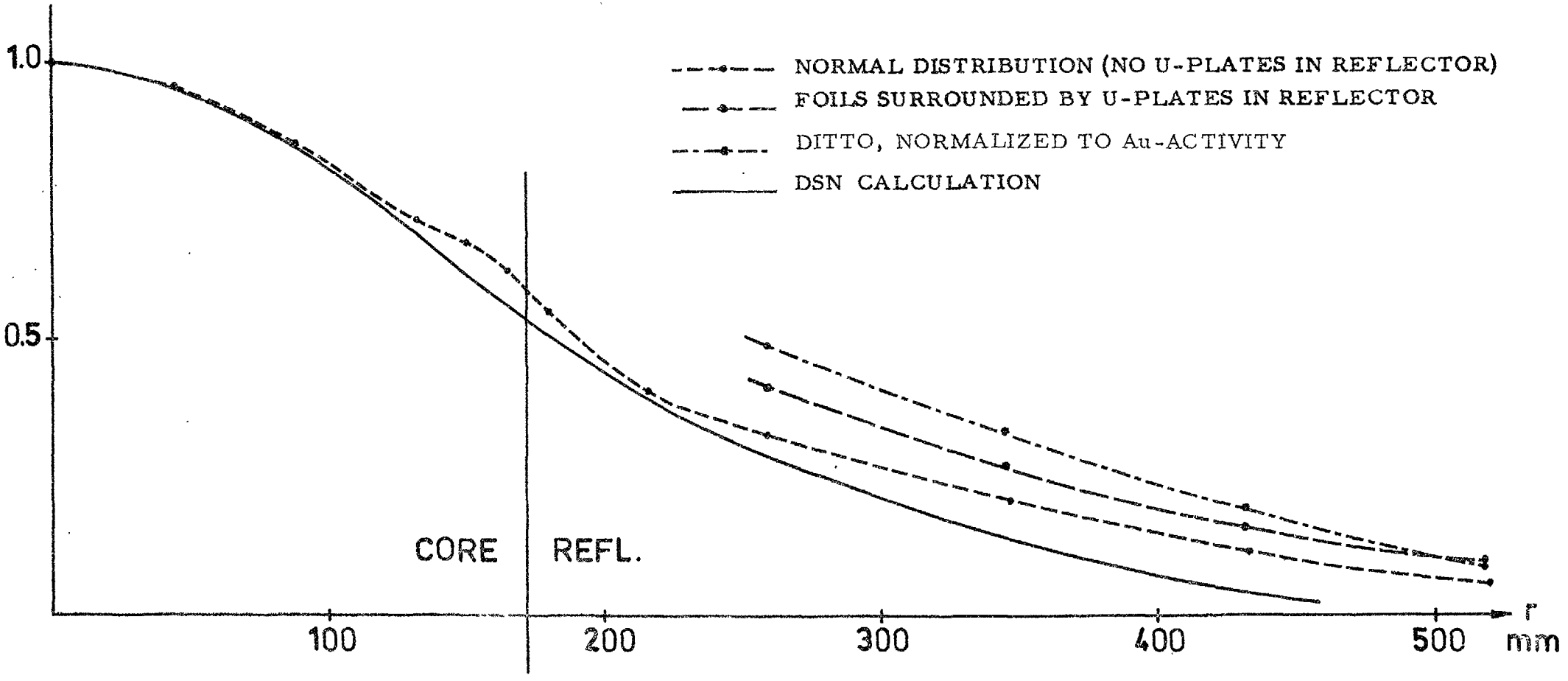

Fig. 13

Cu63(n, γ) reaction rate, radial distribution in assembly 2

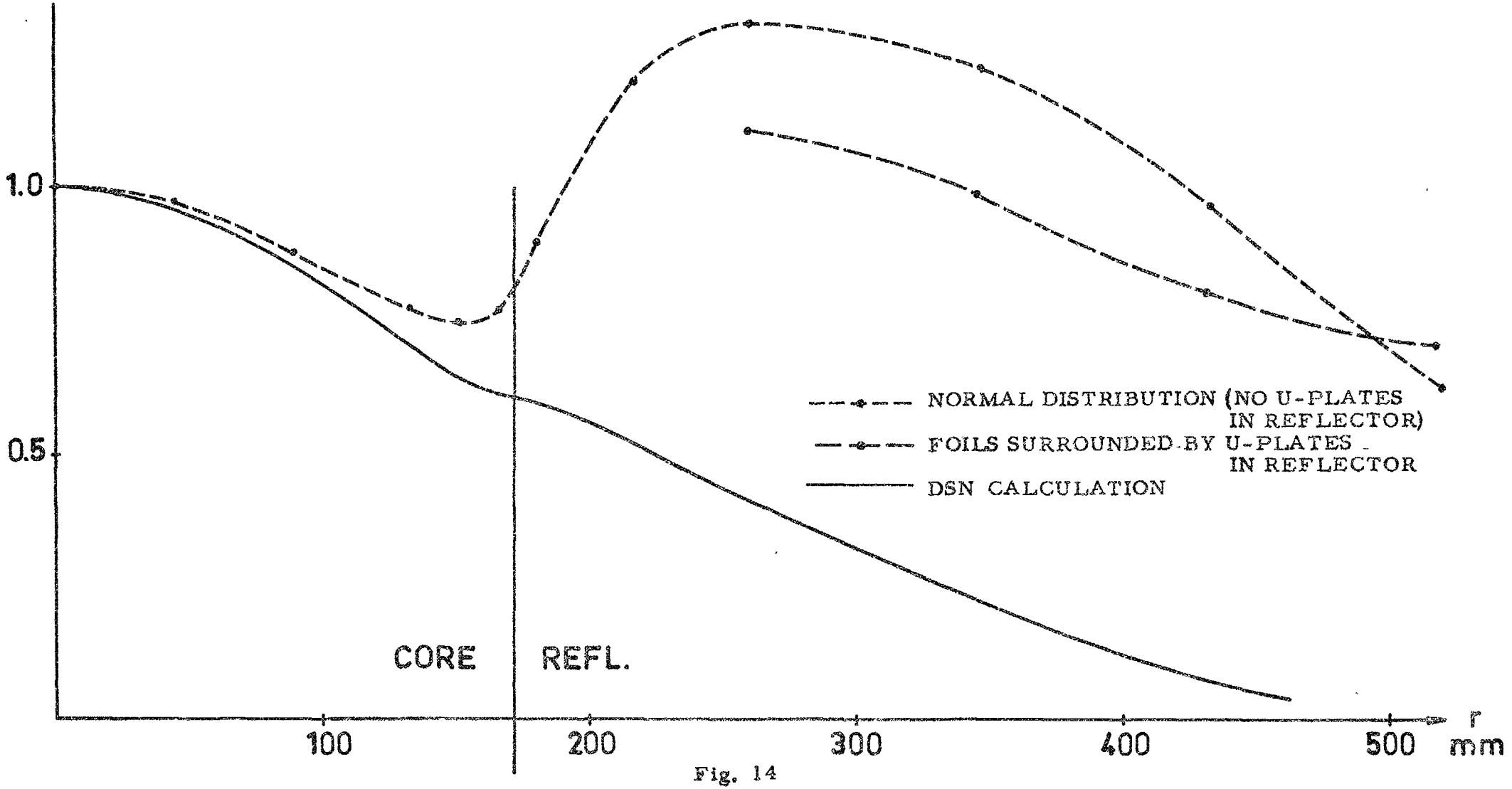

Fig. 14

Au197(n, γ) reaction rate, radial distribution in assembly 2

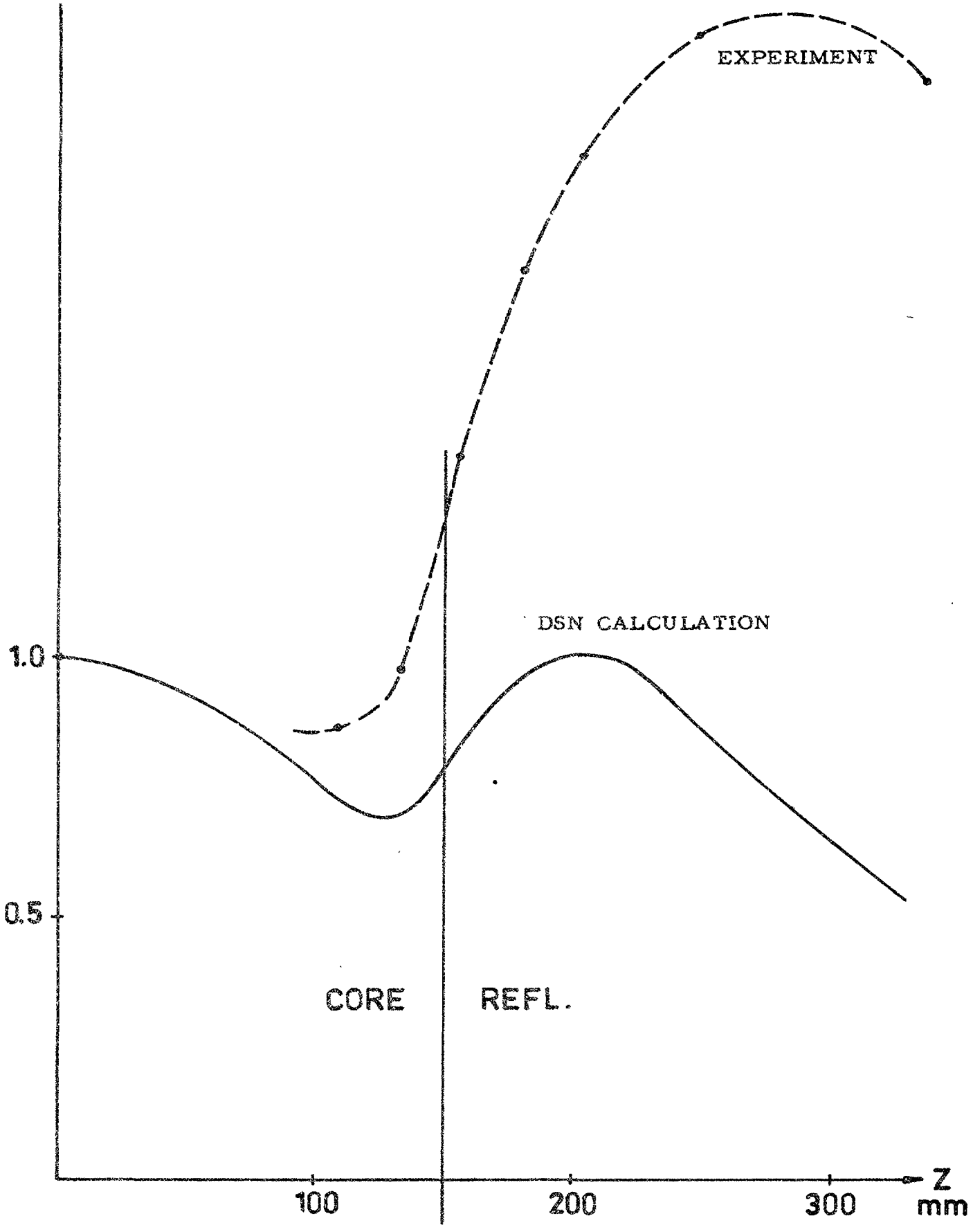

Fig. 15

Mn55(n, γ) reaction rate, axial distribution in assembly 1

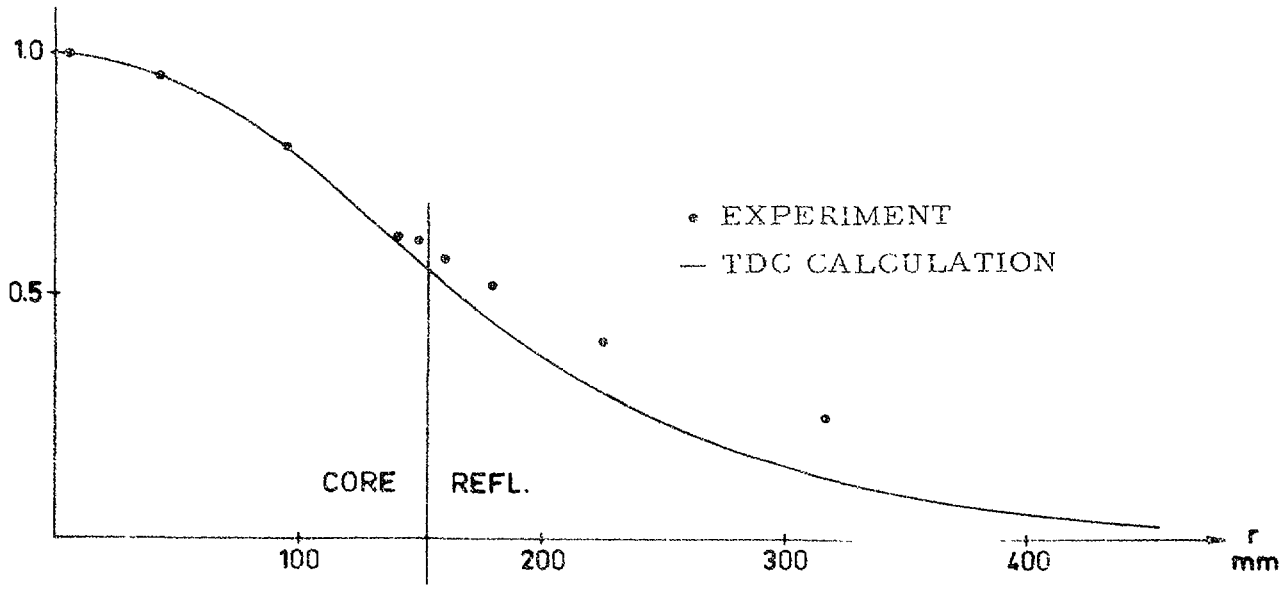

ASSEMBLY 1

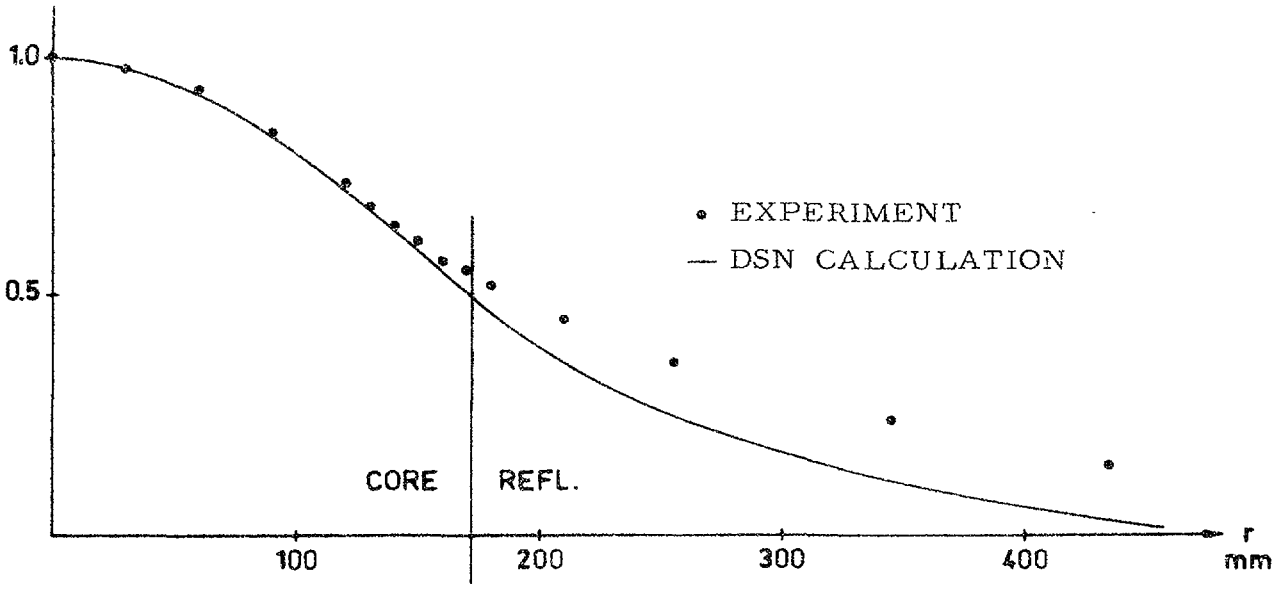

ASSEMBLY 2

Fig. 16

U235 fission rate, radial distribution

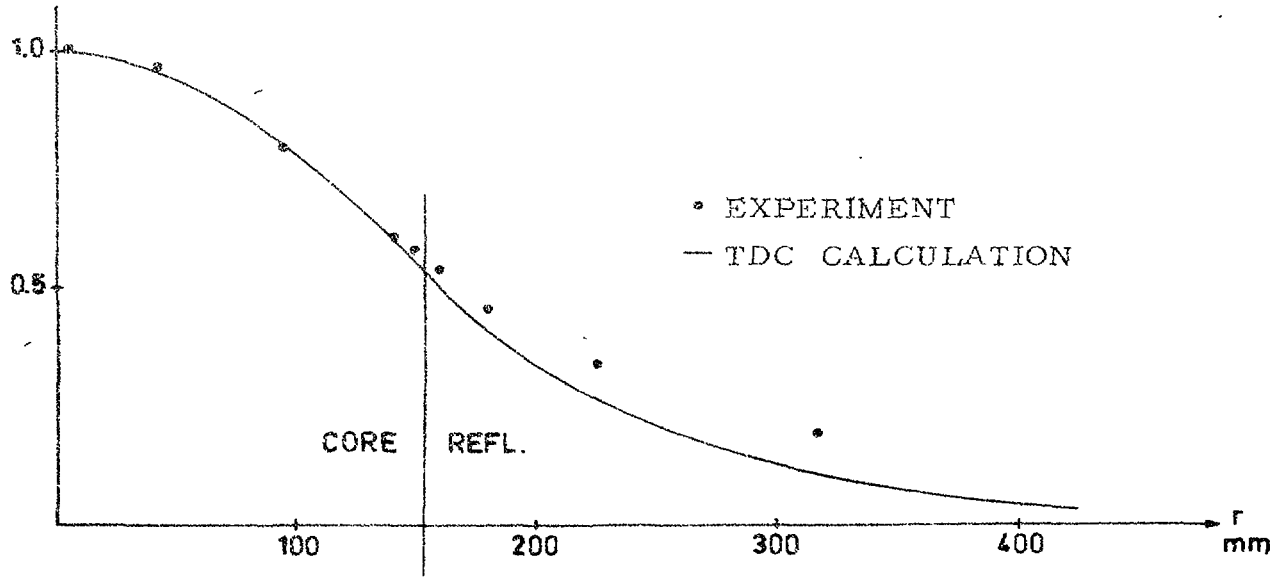

ASSEMBLY 1

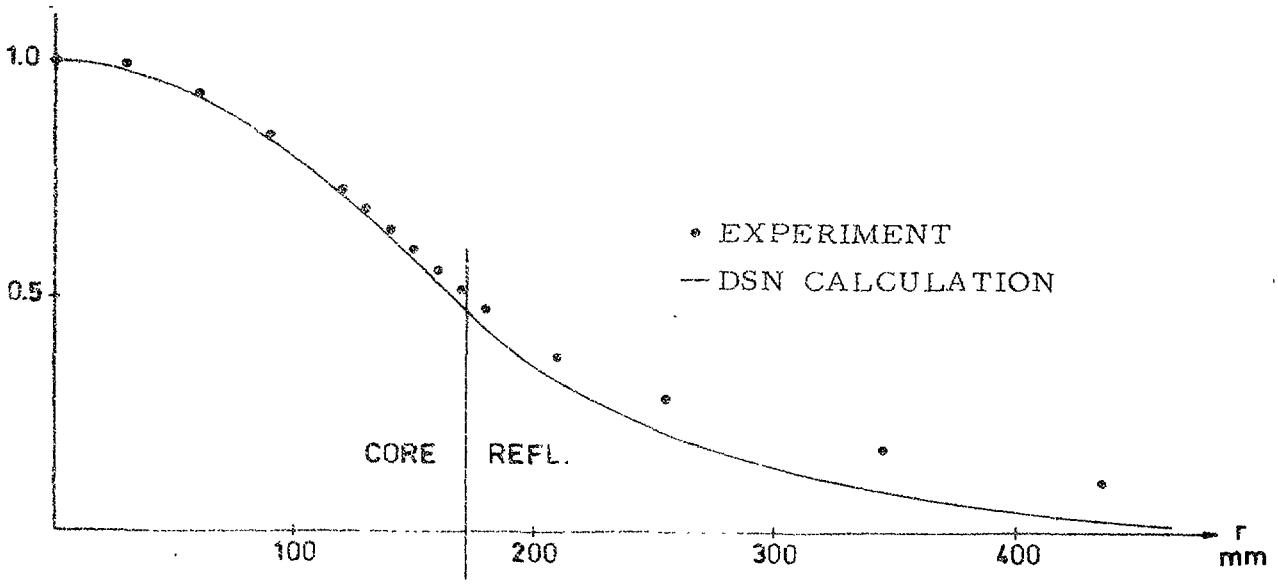

ASSEMBLY 2

Fig. 17

Pu239 fission rate, radial distribution

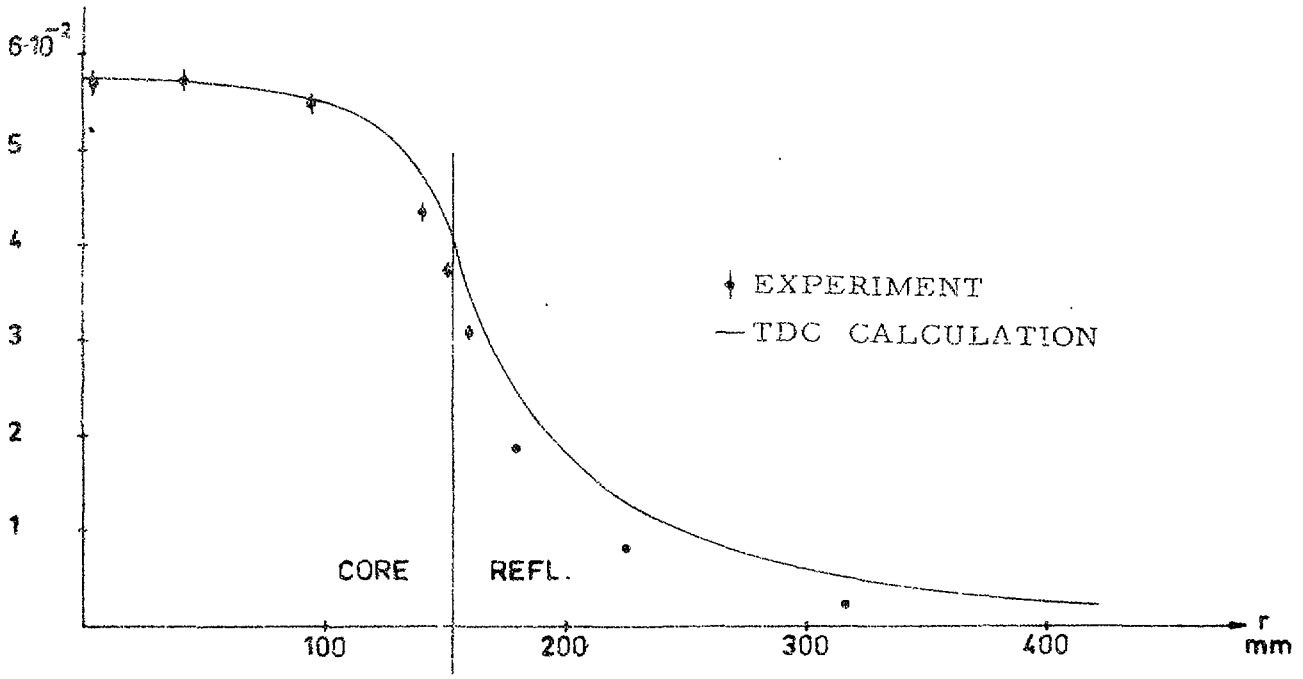

ASSEMBLY 1

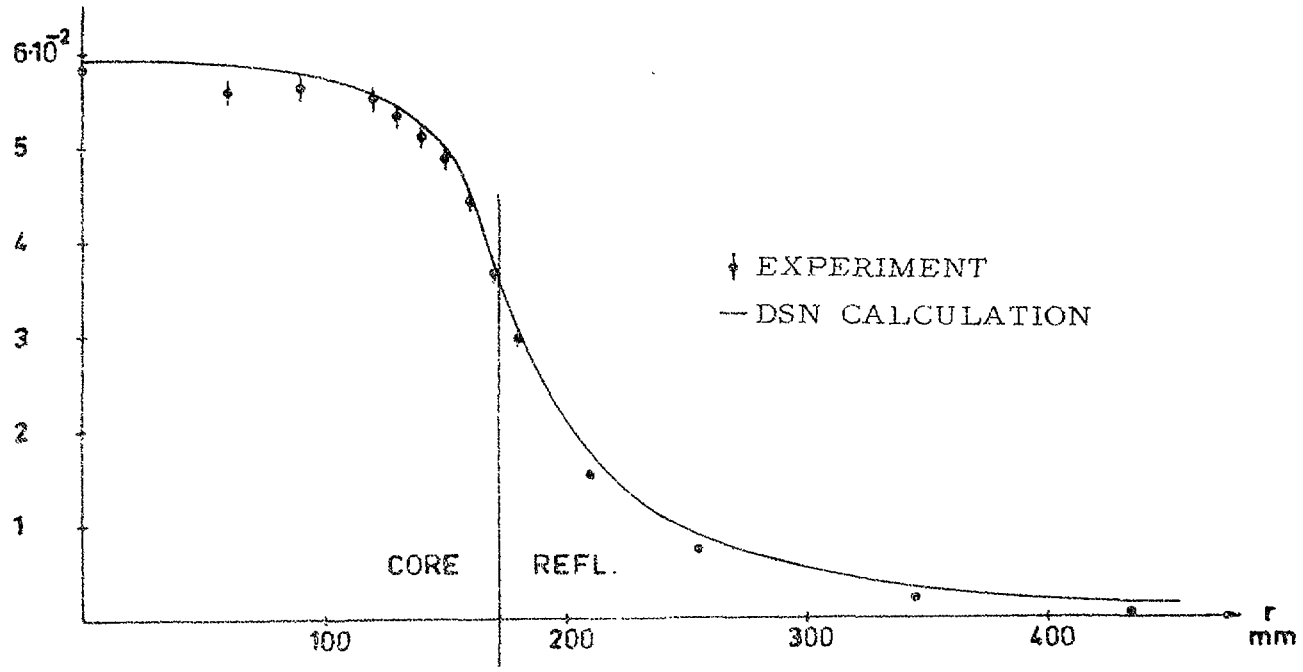

ASSEMBLY 2

Fig. 18

$\frac{U238}{U235}$ fission ratio, radial distribution

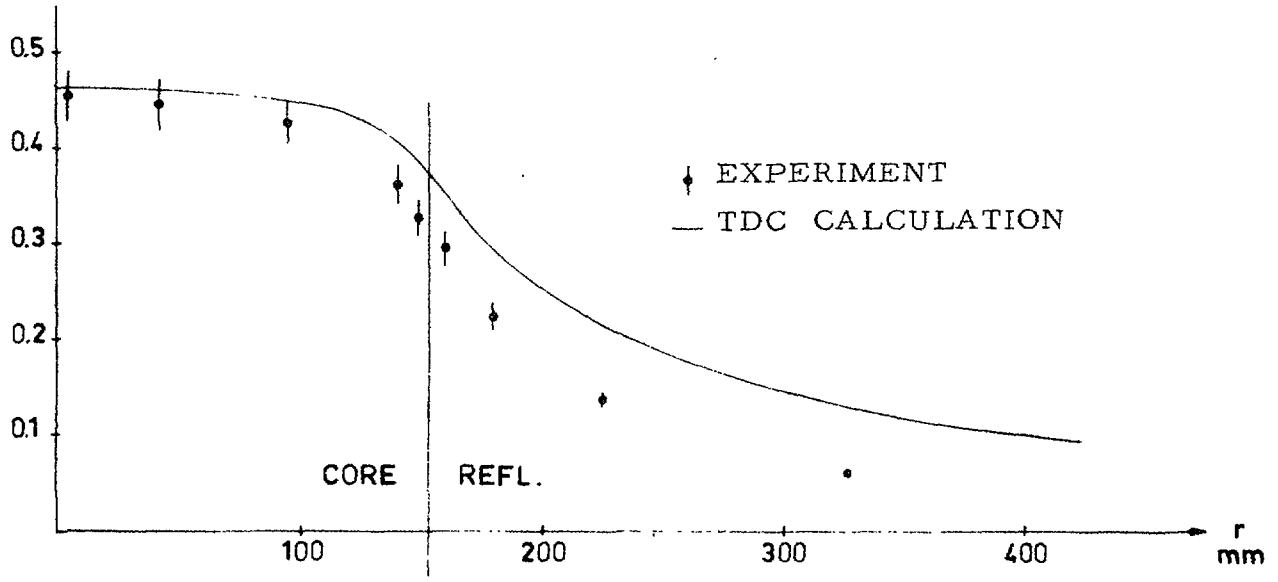

ASSEMBLY 1

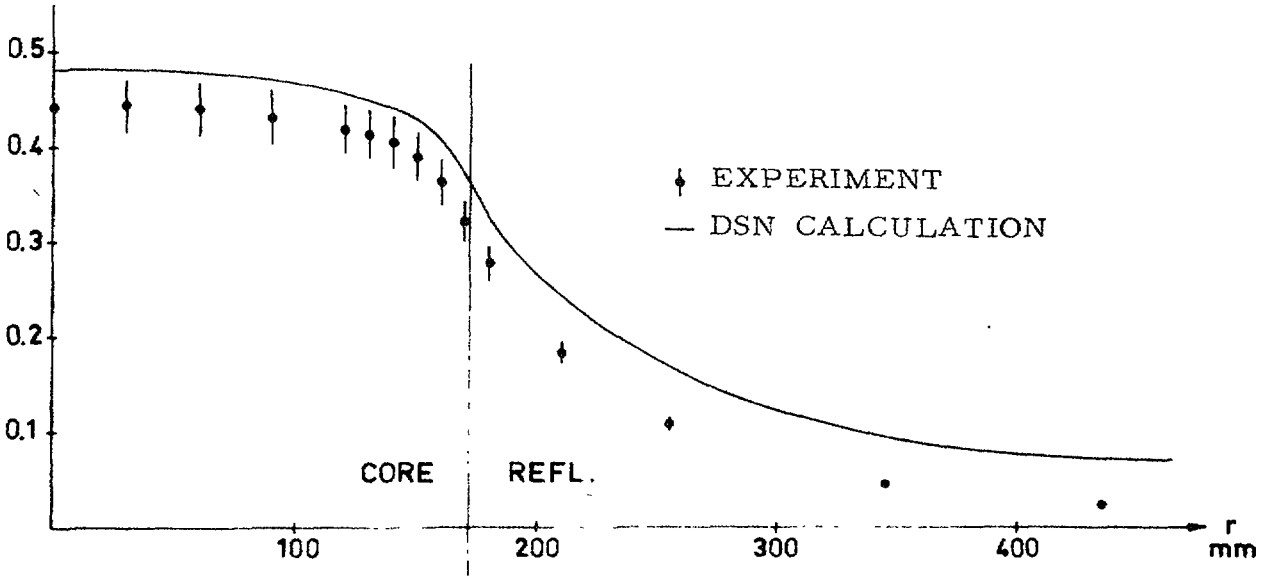

ASSEMBLY 2

Fig. 19

$\frac{Np237}{U235}$ fission ratio, radial distribution

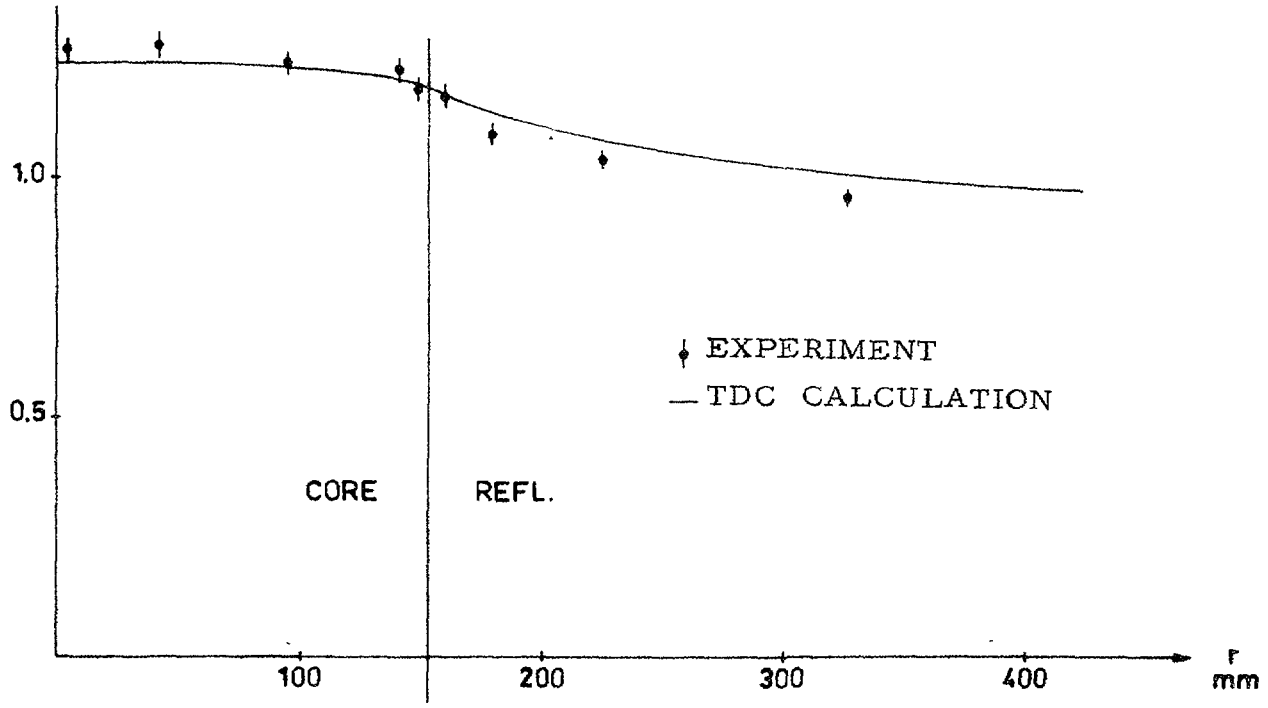

ASSEMBLY 1

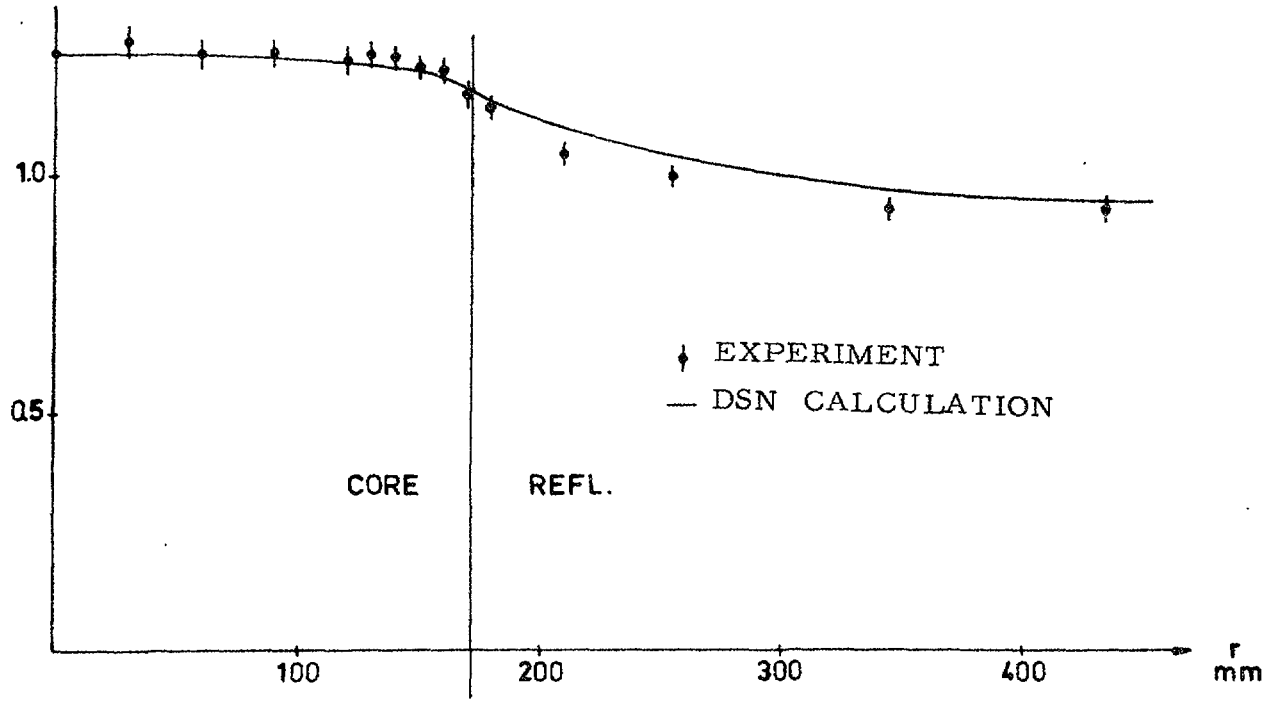

ASSEMBLY 2

Fig. 20

$\frac{Pu239}{U235}$ fission ratio, radial distribution

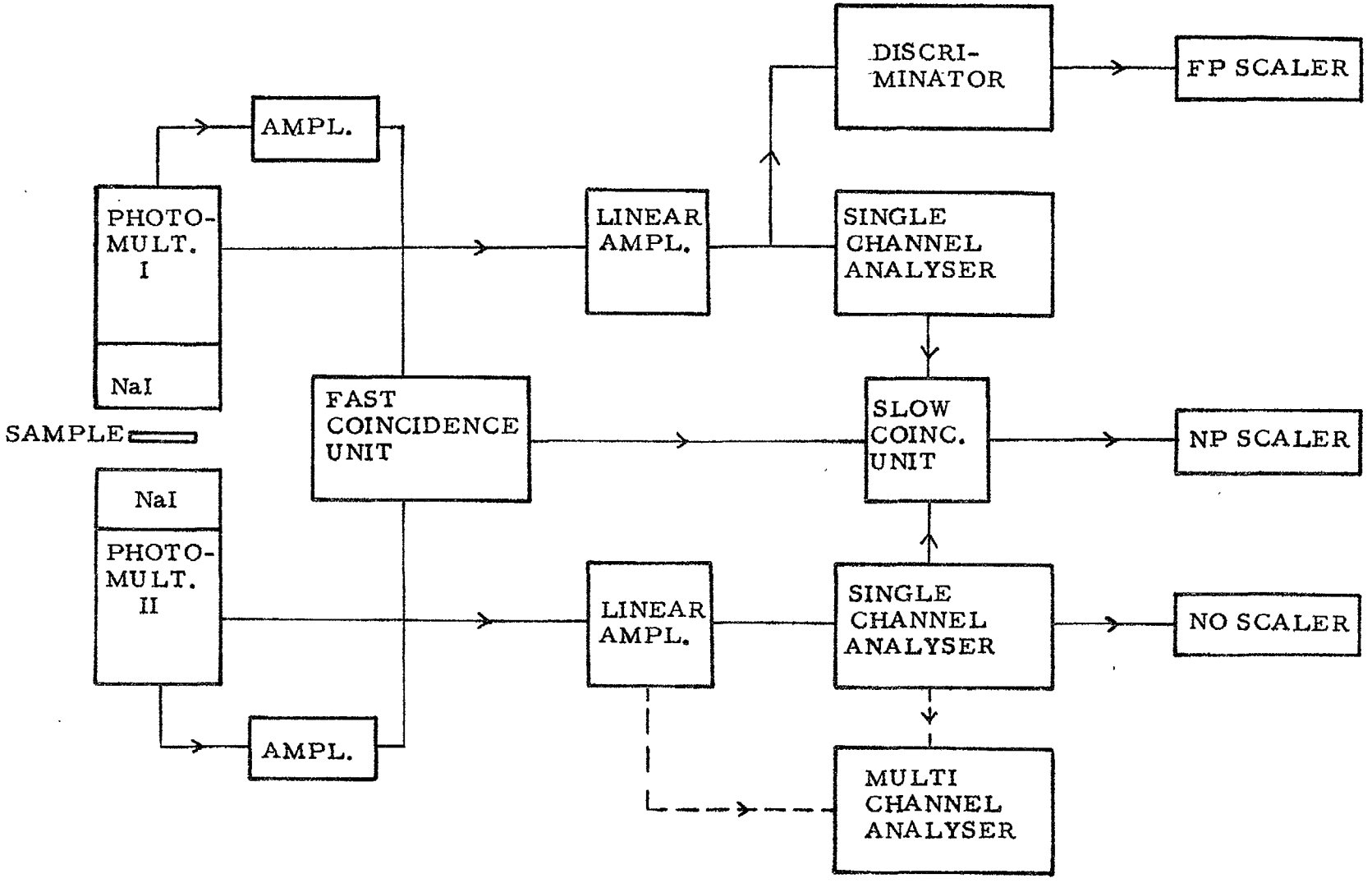

Fig. 21

Fast-slow coincidence apparatus

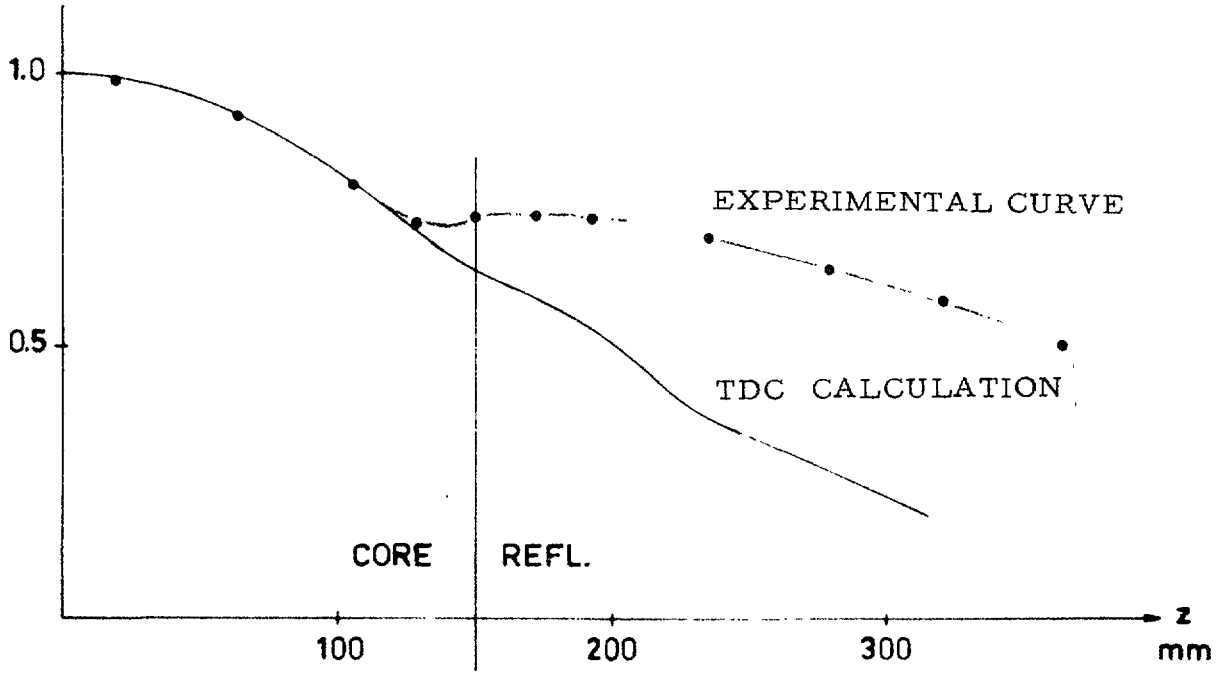

Fig. 22

U238 capture rate, axial distribution in assembly 1

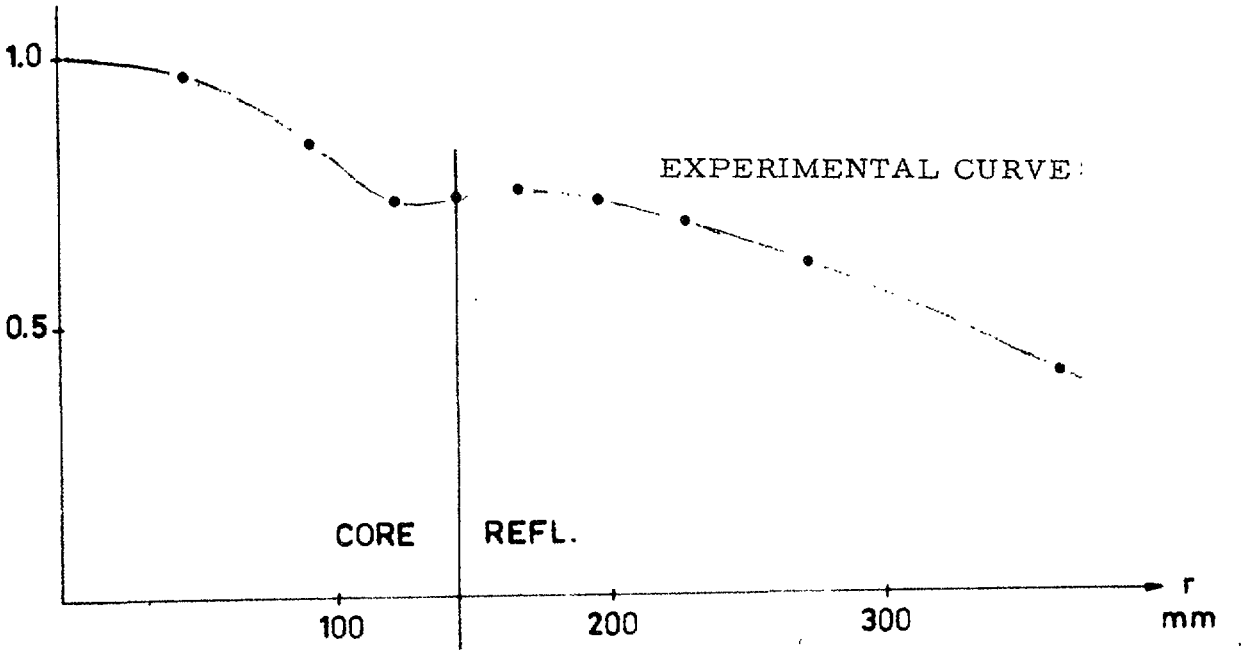

Fig. 23

U238 capture rate, radial distribution in assembly 1

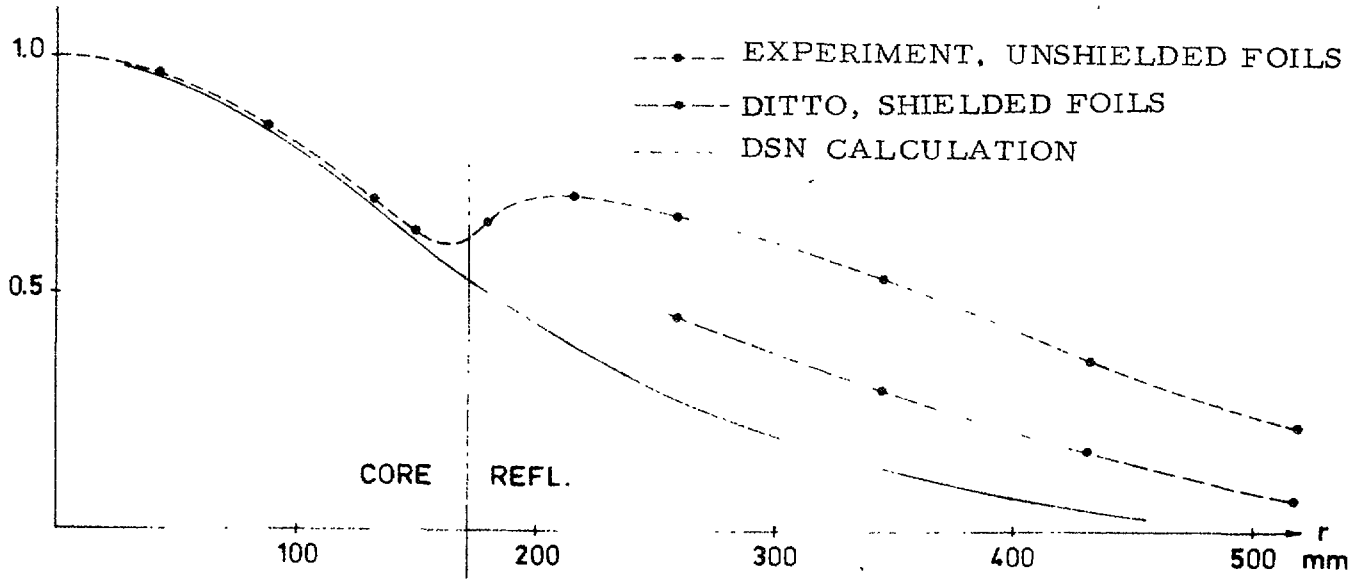

Fig. 24

U238 capture rate, radial distribution in assembly 2

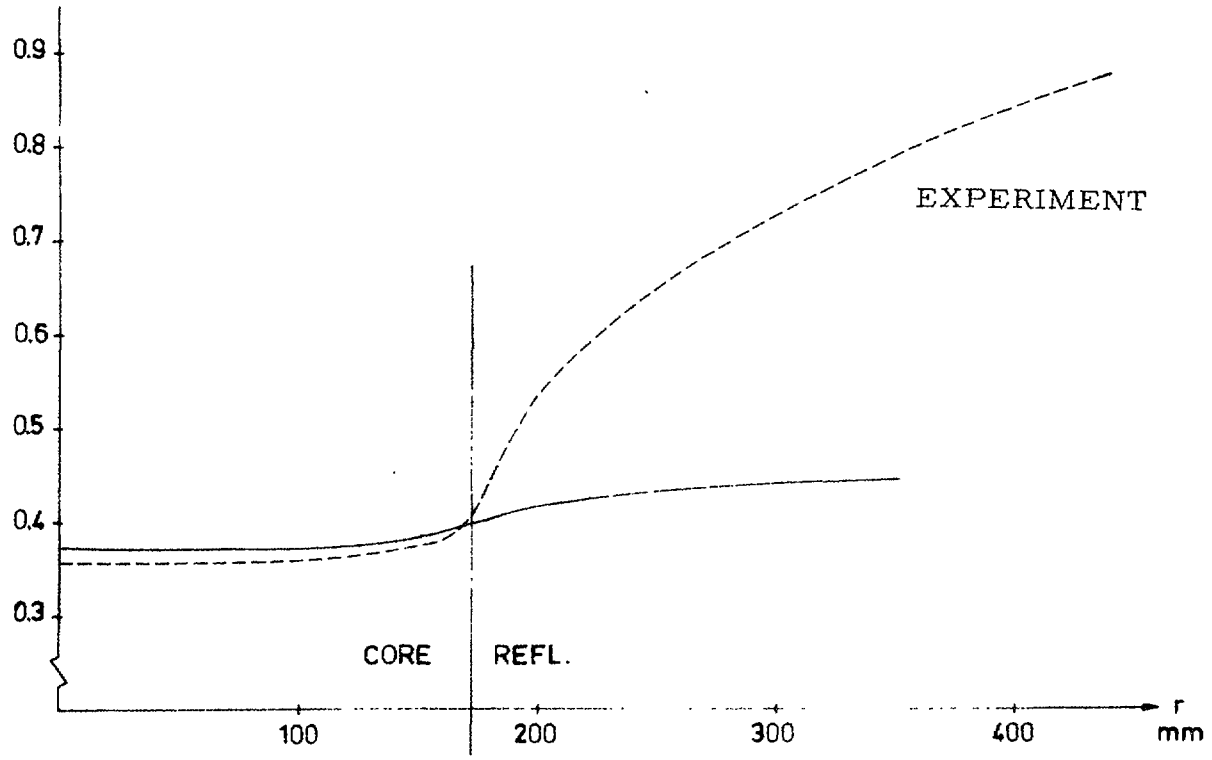

Fig. 25

Distribution of local conversion ratio in assembly 2

LIST OF PUBLISHED AE-REPORTS

1—120. (See the back cover earlier reports.)

121. The transistor as low level switch. By A. Lydén. 1963. 47 p. Sw. cr. 8:—.

122. The planning of a small pilot plant for development work on aqueous reprocessing of nuclear fuels. By T. U. Sjöborg, E. Haeffner and Hultgren. 1963. 20 p. Sw. cr. 8:—.

123. The neutron spectrum in a uranium tube. By E. Johansson, E. Jonsson, M. Lindberg and J. Mednis. 1963. 36 p. Sw. cr. 8:—.

124. Simultaneous determination of 30 trace elements in cancerous and noncancerous human tissue samples with gamma-ray spectrometry. K. Samsahl, D. Brune and P. O. Wester. 1963. 23 p. Sw. cr. 8:—.

125. Measurement of the slowing-down and thermalization time of neutrons in water. By E. Möller and N. G. Sjöstrand. 1963. 42 p. Sw. cr. 8:—.

126. Report an the personell dosimetry at AB Atomenergi during 1962. By K.-A. Edvardsson and S. Hagsgård. 1963. 12 p. Sw. cr. 8:—.

127. A gas target with a tritium gas handling system. By B. Holmqvist and T. Wiedling. 1963. 12 p. Sw. cr. 8:—.

128. Optimization in activation analysis by means of epithermal neutrons. Determination of molybdenum in steel. By D. Brune and K. Jirlow. 1963. 11 p. Sw. cr. 8:—.

129. The P_1-approximation for the distribution of neutrans from a pulsed source in hydrogen. By A. Claesson. 1963. 18 p. Sw. cr. 8:—.

130. Dislocation arrangemants in deformed and neutron irradiated zirconium and zircaloy-2. By R. B. Roy. 1963. 18 p. Sw. cr. 8:—.

131. Measurements of hydrodynamic instabilities, flow oscillatians and burnaut in a natural cirkulation loop. By K. M. Becker, R. P. Mathisen, O. Eklind and B. Norman. 1964. 21 p. Sw. cr. 8:—.

132. A neutron rem counter. By I. O. Andersson and J. Braun. 1964. 14 p. Sw. cr. 8:—.

133. Studies of water by scattering of slow neutrons. By K. Sköld, E. Pilcher and K. E. Larsson. 1964. 17 p. Sw. cr. 8:—.

134. The amounts of As, Au, Br, Cu, Fe, Mo, Se, and Zn in normal and uraemic human whole blood. A comparison by means neutran activation analysis. By D. Brune, K. Samsahl and P. O. Wester. 1964. 10 p. Sw. cr. 8:—.

135. A Monte Carlo method för the analysis of gamma radiation transport from distributed sources in laminated shields. By M. Leimdörfer. 1964. 28 p. Sw. cr. 8:—.

136. Ejection of uranium atoms from UO_2 by fission fragments. By G. Nilsson. 1964. 38 p. Sw. cr. 8:—.

137. Personell neutron monitoring at AB Atomenergi. By S. Hagsgård and C.-O. Widell. 1964. 11 p. Sw. cr. 8:—.

138. Radiation induced precipitation in iron. By B. Solly. 1964. 8 p. Sw. cr. 8:—.

139. Angular distributions of neutrons from (p, n)-reactions in some mirror nuclei. By L. G. Strömberg, T. Wiedling and B. Holmqvist. 1964. 28 p. Sw. cr. 8:—.

140. An extended Greuling-Goertzel approximation with a P_n -appraximation in the angular dependence. By R. Håkanssan. 1964. 21 p. Sw. cr. 8:—.

141. Heat transfer and pressure drop with rough surfaces, a literature survey. By A. Bhattachayya. 1964. 78 p. Sw. cr. 8:—.

142. Radiolysis of aqueous benzene solutions. By H. Christensen. 1964. 50 p. Sw. cr. 8:—.

143. Cross section measurements for some elements suited as thermal spectrum indicatars: Cd, Sm, Gd and Lu. By E. Sokolowski, H. Pekarek and E. Jonsson. 1964. 27 p. Sw. cr. 8:—.

144. A direction sensitive fast neutron monitor. By B. Antolkovic, B. Halmqvist and T. Wiedling. 1964. 14 p. Sw. cr. 8:—.

145. A user's manual for the NRN shield design methad. By L. Hjärne. 1964. 107 p. Sw. cr. 10:—.

146. Cancentration of 24 trace elements in human heart tissue determined by neutron activation analysis. By P. O. Wester. 1964. 33 p. Sw. cr. 8:—.

147. Report on the personnel Dosimetry at AB Atomenergi during 1963. By K.-A. Edvardsson and S. Hagsgård. 1964. 16 p. Sw. cr. 8:—.

148. A calculation of the angular moments of the kernel for a monatomic gas scatterer. By R. Håkansson. 1964. 16 p. Sw. cr. 8:—.

149. An anion-exchange method for the separation of P-32 activity in neutron-irradited biological material. By K. Samsahl. 1964. 10 p. Sw. cr 8:—.

150. Inelastic neutron scattering cross sections of Cu^{63} and Cu^{65} in the energy region 0.7 to 1.4 MeV. By B. Holmqvist and T. Wiedling. 1964. 30 p. Sw. cr. 8:—.

151. Determination of magnesium in needle biopsy samples of muscle tissue by means of neutron activation analysis. By D. Brune and H. E. Sjöberg. 1964. 8 p. Sw. cr. 8:—.

152. Absolute El transition probabilities in the dofermed nuclei Yb^{177} and Hf^{179}. By Sven G. Malmskog. 1964. 21 p. Sw. cr. 8:—.

153. Measurements of burnout conditions for flow of boiling water in vertical 3-rod and 7-rod clusters. By K. M. Becker, G. Hernborg and J. E. Flinta. 1964. 54 p. Sw. cr. 8:—.

154. Integral parameters of the thermal neutron scattering law. By S. N. Purohit. 1964. 48 p. Sw. cr. 8:—.

155. Tests of neutron spectrum calculations with the help of foil measurments in a D_2O and in an H_2O-moderated reactor and in reactor shields of concrete and iron. By R. Nilsson and E. Aalto. 1964. 23 p. Sw. cr. 8:—.

156. Hydrodynamic instability and dynamic burnout in natural circulation two-phase flow. An experimental and theoretical study. By K. M. Becker. S. Jahnberg, I. Haga, P. T. Hansson and R. P. Mathisen. 1964. 41 p. Sw. cr. 8:—.

157. Measurements of neutron and gamma attenuation in massive laminated shields of concrete and a study of the accuracy of some methods of calculatian. By E. Aalto and R. Nilsson. 1964. 110 p. Sw. cr. 10:—.

158. A study of the angular distributions of neutrons from the Be^9 (p,n) B^9 reaction at low proton energies. By. B. Antolkovic', B. Holmqvist and T. Wiedling. 1964. 19 p. Sw. cr. 8:—.

159. A simple apparatus for fast ion exchange separations. By K. Samsahl. 1964. 15 p. Sw. cr. 8:—.

160. Measurements of the Fe^{54} (n, p) Mn^{54} reaction cross section in the neutron energy range 2.3—3.8 MeV. By A. Lauber and S. Malmskog. 1964. 13 p. Sw. cr. 8:—.

161. Comparisons of measured and calculated neutron fluxes in laminated iron and heavy water. By. E. Aalto. 1964. 15 p. Sw. cr. 8:—.

162. A needle-type p-i-n junction semiconductor detector for in-vivo measurement of beta tracer activity. By A. Lauber and B. Rosencrantz. 1964. 12 p. Sw. cr. 8:—.

163. Flame spectro photometric determination of strontium in water and biological material. By G. Jönsson. 1964. 12 p. Sw. cr. 8:—.

164. The solution of a velocity-dependent slawing-down problem using case's eigenfunction expansion. By A. Claesson. 1964. 16 p. Sw. cr. 8:—.

165. Measurements of the effects of spacers on the burnout conditions for flow of boiling water in a vertical annulus and a vertical 7-rod cluster. By K. M. Becker and G. Hernberg. 1964. 15 p. Sw. cr. 8:—.

166. The transmissian of thermal and fast neutrons in air filled annular ducts through slabs of iron and heavy water. By J. Nilsson and R. Sandlin. 1964. 33 p. Sw. cr. 8:—.

167. The radio-thermoluminescense of $CaSO_4$: Sm and its use in dosimetry. By B. Bjärngard. 1964. 31 p. Sw. cr. 8:—.

168. A fast radiochemical method for the determination of same essential trace elements in biology and medicine. By K. Samsahl. 1964. 12 p. Sw. cr. 8:—.

169. Concentration of 17 elements in subcellular fractions of beef heart tissue determined by neutron activation analysis. By P. O. Wester. 1964. 29 p. Sw. cr. 8:—.

170. Formation of nitrogen-13, fluorine-17, and fluorine-18 in reactor-irradiated H_2O and D_2O and applications to activation analysis and fast neutron flux monitoring. By L. Hammor and S. Forsén. 1964. 25 p. Sw. cr. 8:—.

171. Measurements on background and fall-out radioactivity in samples from the Baltic bay of Tvären, 1957—1963. By P. O. Agnedal. 1965. 48 p. Sw. cr. 8:—.

172. Recoil reactions in neutron-activation analysis. By D. Brune. 1965. 24 p. Sw. cr. 8:—.

173. A parametric study of a constant-Mach-number MHD generator with nuclear ionization. By J. Braun. 1965. 23 p. Sw. cr. 8:—.

174. Improvements in applied gamma-ray spectrometry with germanium semiconductor dector. By D. Brune, J. Dubois and S. Hellström. 1965. 17 p. Sw. cr. 8:—.

175. Analysis of linear MHD power generators. By E. A. Witalis. 1965. 37 p. Sw. cr. 8:—.

176. Effect of buayancy on forced convection heat tranfer in vertical channels — a literature survey. By A. Bhattacharyya. 1965. 27 p. Sw. cr. 8:—.

177. Burnout data for flow of boiling water in vertical round ducts, annuli and rod clusters. By K. M. Becker, G. Hernborg, M. Bade and O. Erikson. 1965. 109 p. Sw. cr. 8:—.

178. An analytical and experimental study of burnout conditions in vertical round ducts. By K. M. Becker. 1965. 161 p. Sw. cr. 8:—.

179. Hindered El transitions in Eu^{155} and Tb^{161}. By S. G. Malmskog. 1965. 19 p. Sw. cr. 8:—.

180. Photomultiplier tubes for low level Cerenkov detectors. By O. Strindehag. 1965. 25 p. Sw. cr. 8:—.

181. Studies of the fission integrals of U235 and Pu239 with cadmium and boron filters. By E. Hellstrand. 1965. 32 p. Sw. cr. 8:—.

182. The handling of liquid waste at the research statian of Studsvik, Sweden. By S. Lindhe and P. Linder. 1965. 18 p. Sw. cr. 8:—.

183. Mechanical and instrumental experiences from the erection, commissioning and operation of a small pilot plant for development work on aqueous reprocessing of nuclear fuels. By K. Jönsson. 1965. 21 p. Sw. cr. 8:—.

184. Energy dependent removal cross-sections in fast neutron shielding theory. By H. Grönraos. 1965. 75 p. Sw. cr. 8:—.

185. A new method for predicting the penetration and slowing-down of neutrons in reactor shields. By L. Hjärne and M. Leimdörfer. 1965. 21 p. Sw. cr. 8:—.

186. An electron microscope study of the thermal neutron induced loss in high temperature tensile ductility of Nb stabilized austenitic steels. By R. B. Roy. 1965. 15 p. Sw. cr. 8:—.

187. The non-destructive determination of burn-up means of the Pr-144 2.18 MeV gamma activity. By R. S. Forsyth and W. H. Blackadder. 1965. 22 p. Sw. cr. 8:—.

188. Trace elements in human myocardial infarction determined by neutron activation analysis. By P. O. Wester. 1965. 34 p. Sw. cr. 8:—.

189. An electromagnet for precession of the polarization of fast-neutrons. By O. Aspelund, J. Bäckman and G. Trumpy. 1965. 28 p. Sw. cr. 8:—.

190. On the use of importance sampling in particle transport problems. By B. Eriksson. 1965. 27 p. Sw. cr. 8:—.

191. Trace elements in the conductive tissue of beef heart determined by neutron activation analysis. By P. O. Wester. 1965. 19 p. Sw. cr. 8:—.

192. Radiolysis of aqueous benzene solutions in the presence of inorganic oxides. By H. Christensen. 12 p. 1965. Sw. cr. 8:—.

193. Radiolysis of aqueous benzene solutions at higher temperatures. By H. Christensen. 1965. 14 p. Sw. cr. 8:—.

194. Theoretical work for the fast zero-power reactor FR-0. By H. Häggblom. 1965. 46 p. Sw. cr. 8:—.

195. Experimental studies on assemblies 1 and 2 of the fast reactor FR0. Part 1. By T. L. Andersson, E. Hellstrand, S-O. Londen and L. I. Tirén. 1965. 45 p. Sw. cr. 8:—.

Förteckning över publicerade AES-rapporter

1. Analys medelst gamma-spektrometri. Av D. Brune. 1961. 10 s. Kr 6:—.
2. Beströlningsförändringar och neutronatmosfär i reaktortrycktankar — några synpunkter. Av M. Grounes. 1962. 33 s. Kr 6:—.
3. Studium av sträckgränsen i mjukt stål. Av G. Östberg och R. Attermo. 1963. 17 s. Kr 6:—.
4. Teknisk upphondling inom reaktorområdet. Av Erik Jonson. 1963. 64 s. Kr 8:—.
5. Agesta Kraftvärmeverk. Sammanställning av tekniska data, beskrivningar m. m. för reaktordelen. Av B. Lilliehöök. 1964. 336 s. Kr 15:—.

Additional copies available at the library of AB Atomenergi, Studsvik, Nyköping, Sweden. Transparent microcards of the reports are obtainable through the International Documentation Center, Tumba, Sweden.

EOS-tryckerierna, Stockholm 1965